11 Ultraviolet Radiation and Its Interaction with Air Pollution

William F. Barnard[1] and Brian N. Wenny[2]

[1] North Carolina State University, Department of Marine, Earth, and Atmospheric Sciences, Campus Box 8208
Raleigh, North Carolina 27695-8208, USA
E-mail: SBarn46193@aol.com
[2] MODIS Characterization Support Team (MCST)
Sigma Space Corp.
10210 Greenbelt Road, Suite 500
Lanham, MD 20706
E-mail: brian.wenny@gmail.com

Abstract This chapter contains the methodology, along with study examples, that show the types of interactions that the sun's ultraviolet (UV) spectrum has with the various pollutants in the earth's atmosphere, predominantly those in the troposphere. In the context of this chapter, the absorption of UV by gaseous pollutants (stratospheric ozone is not considered a pollutant) has been observed to present a much smaller problem than originally thought. Additionally, aerosols, particularly black carbon, play a much larger role. One must keep in mind that only two studies are presented here in determining site specific UV transmissions to the surface. Each site has its own variables, not the least of which is the differing combinations of scattering and absorbing aerosols. There is a great need to characterize more sites and identify aerosol types according to their chemical species and by doing so, relate the species to the single scatter albedo and aerosol optical depth. It will then become possible to transfer this ground-based knowledge to satellite observation points so that predictions of surface UV can become more accurate in protecting our environment.

Keywords aerosols, single scatter albedo, black carbon, atmospheric optical depth, particulate scattering and absorption

11.1 Introduction

To attempt to understand this problem, certain concepts and definitions need to be laid out at the beginning to better understand the complexity of this subject.

Air pollution, optics, radiative transfer methodology, information on atmospheric construction, along with models and statistics are all utilized in this chapter to show the complexity of the interaction of ultraviolet UV radiation with air pollution. Because of the nature of UV radiation and its interaction with the atmosphere and its constituents, certain parameters and their known effects on the UV will be explained first so that the reader gets a perspective of the variations that the role of air pollution can play in the earth's UV field. UV radiation, while making up only 1.5% of the total radiation that the earth receives, is the most energetic. Its shorter wavelengths make it highly susceptible for interception by almost anything in its path. Since the earth's climate is constantly changing, the UV that reaches the surface is also changing.

11.1.1 Factors Affecting UV Flux at the Earth's Surface

- Solar zenith angle
- Stratospheric ozone
- Cloud cover
- Atmospheric density
- Air pollution (gases and aerosols)

11.1.1.1 Solar Zenith Angle

If one goes from New York to the Bahamas for a winter vacation, there is a known increase in the UV just from the change in latitude, and thus, the solar zenith angle (SZA) (Fig. 11.1). The same occurs on a summer's day where the solar angle (dependant on latitude) can change dramatically. Ultraviolet radiation around solar noon has its shortest path length to the surface and thus, its greatest intensities. To further increase the UV exposure, one only needs to go to a higher altitude in a lower latitude situation. Here, there is less atmosphere to scatter and absorb the UV and generally, as in the case of Mauna Loa, HI, a very clean environment in which to calibrate the very monitors that measure the surface UV in the more polluted regions of the earth. Ultraviolet-B (UV-B) radiation (280 nm – 320 nm)

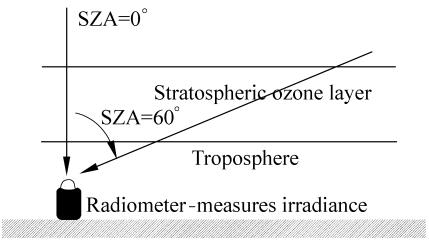

Figure 11.1 Solar zenith angle

comprises roughly 1.5% of the total extraterrestrial solar irradiance and 0.5% of incident irradiance at the earth's surface. Ultraviolet-A (UV-A) radiation encompasses the wavelength region from 320 nm – 400 nm. Ultraviolet radiation has both a daily component that resembles the bell shape distribution curve and a seasonal component that can be expressed with a combination of sine and cosine functions dependant on the Julian date. The daily component's shape is dependant on the wavelength. The shorter wavelengths of 300 nm – 310 nm are generally not observed until the sun has risen past 9:00 a.m. local time in the summer. The longer wavelengths 360 nm – 400 nm exist in the daylight sky from sunrise until sunset.

11.1.1.2 Stratospheric Ozone

The one main absorbing parameter that must be kept constant if the effects of air pollution are being determined is the known interaction of the UV with the stratospheric ozone. The UV absorbed in this layer is the predominant factor affecting the transmission to the earth's surface. Statistical correlations of surface measured UV with variations in this layer of ozone correlate well above the $r = 0.90$ level. The importance of ozone as a regulator of UV stems from strong absorption characteristics over the entire ultraviolet region. Ozone exists in two places in the atmosphere; one is where it is supposed to be to protect life on earth: the stratosphere, and the other, the troposphere, where it is a pollutant that can cause severe health problems. Both ozone areas require high energy UV radiation for creation, but in entirely different ways. In one case it is the primary absorber of UV radiation. In the other, UV creates the tropospheric ozone. Stratospheric ozone is produced by a series of reactions with molecular oxygen and singlet oxygen in the presence of high energy UV radiation, UV-C (200 nm – 280 nm). It is primarily produced over the equatorial regions and is slowly transported poleward. The total column ozone (stratospheric and tropospheric) can comprise a major UV absorber under highly polluted conditions. In the troposphere the UV can create the very gas that helps in its own attenuation. Although in general, as will be shown later, the tropospheric gases play a minor UV absorption role in comparison to other aerosol pollutants.

Stratospheric ozone absorbs all of the UV-C radiation. Tropospheric ozone makes up only a small portion of the total column ozone, usually less than 10%. The path length of the stratosphere is much longer than that of the troposphere, but the higher density of the troposphere and its increasing scattering capabilities are believed to enhance the absorptive powers of this region (Bruhl and Crutzen, 1989). Tropospheric ozone in urban/industrialized regions may reduce the surface UV by 3% to 15% as estimated by Frederick et al. (1993) and Ma and Guicherit (1997). Under clear sky conditions total ozone column variations cause the largest variations in UV transmission and has been the focus of numerous studies (e.g., McKenzie et al., 1991; Kerr and McElroy, 1993; Bojkov et al., 1995; Mims et al., 1995;

Varotsos and Kondratyev, 1995; Fioletov and Evans, 1997). This relationship is demonstrated in Fig. 11.2, which depicts the calculated clear-sky spectral UV irradiance for two total column amounts, 200 Dobson Units (DU) and 400 DU, for Raleigh, NC, during the summer at high solar elevation.

It is apparent that a decrease in the total ozone column substantially increases the surface UV-B irradiance over the erythemally important wavelengths. The human skin has a response curve to solar radiation. The particular portion of the sun's spectral region, which is in the UV, causes redness of the skin and is the erythemal region.

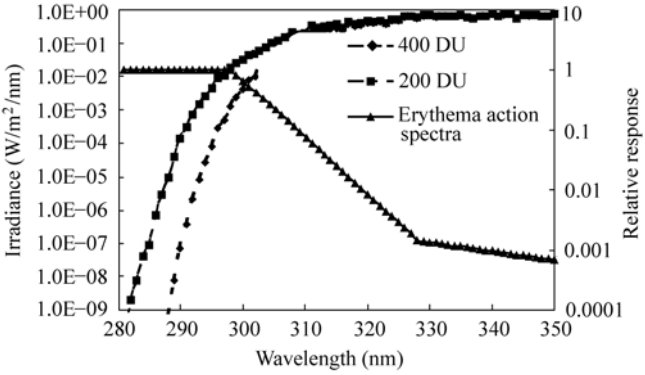

Figure 11.2 UV spectral changes for 200 DU change in stratospheric ozone

11.1.1.3 Cloud Cover

Cloud cover can wreak havoc for making UV measurements. They generally reduce the UV radiation, but it has been shown, Estupinan et al. (1996), and Schafer et al. (1996), that clouds can actually enhance the surface levels by as much as 10%−15%. The physical and chemical makeup of clouds (e.g., thickness, total percent coverage, droplet size distribution, chemical composition, and presence of interstitial absorbing aerosols) causes the cloud's effect on the UV to be highly variable; not only with time, but also with areas of differing pollutant characteristics. Frequently the clouds will act to purge the atmosphere of certain hygroscopic pollutants and in doing so, will alter the atmospheric albedo to reflect UV back to space.

The cloud/physics/chemistry/thermodynamics are not completely understood. Cloud systems vary widely across the world and are dependant upon the cloud type and whether or not they are formed over land or ocean. In one case, they are frequently formed over land where anthropogenic sources have generated thousands of CCN (cloud condensation nuclei) per cubic centimeter, but yet once they are formed (the CCN are hygroscopic, so they collect water vapor as they grow), they become great scavengers of pollution, absorbing the gaseous versions of sulfur

dioxide (SO_2), nitrogen dioxide (NO_2), and ozone (O_3). They may also collect many hydrocarbons, not particularly in solution, but on the droplet surface.

Cloud droplets are formed by condensing water vapor on cloud condensation nuclei. Sizes of these nuclei range from the Aitken nuclei at 0.001 μm up through the large and giant nuclei at 2.0 μm. The smaller nuclei have a much higher concentration in the atmosphere and give rise to clouds with much higher droplet concentrations. These clouds have a higher albedo and provide a cooling effect for the earth's surface by reflecting much of the sunlight back into space. The cloud droplet spectrum broadens as the cloud gets older. For cumulus clouds, this can be caused by collisions and coalescing, condensation and evaporation, turbulence effects, and the mixing of cloud parcels with different histories.

Continental aerosols contain higher concentrations of CCN and thus, cause a different cloud structure over land than over the ocean. The ocean clouds have a broader size distribution of droplet sizes ranging from approximately 6 μm to 45 μm. Droplet counts are in the 35 droplets per cubic centimeter range. However, continental clouds have a narrow size range, 5 μm − 20 μm, but a much higher concentration of approximately 210 droplets/cm^3.

Stratus clouds seem to have the most effect on the radiative transfer and the radiation balance, but don't seem to be studied to the extent that cumulus clouds are. Wind velocities in the two types differ considerably. Cumulus clouds contain updrafts that measure in the meters/second range, while the stratus cloud's wind velocities are in tens of centimeters per second. This is also correlated to the extensive coverage of either type of cloud. Stratus clouds extend coverage over tens of km, while cumulus clouds are generally localized events covering just a few kilometers.

Droplet sizes and growth are different in the two types. Stratus cloud droplets are primarily formed through condensation and their growth processes are largely caused by condensation. The droplets enlarge monotonically with height. The droplet size spectra are narrow as compared to the cumulus. This is caused, in part, by these clouds being contained or height inhibited by an inversion layer just above them. This inhibits further vertical growth of both the cloud and the droplets within.

In the stratus case, there is mixing and partial evaporation at the cloud top causing cooling. Radiative cooling also occurs at the cloud top, as discussed earlier, which causes pockets of colder air to fall through the cloud. These clouds can also contain areas of super cooled droplets. Precipitation is more likely to occur if the cloud is thick and contains ice. The probability of precipitation increases with a combination of cloud age, temperature, and vertical extent. In a cumulus cloud, all three of these exist and are related to cloud thickness. Continental clouds must be thicker than maritime clouds for the same probability of precipitation. The fewer droplets in the maritime clouds are larger and can collide and coalesce with each other more readily than the smaller drops in the continental clouds to form precipitation. Less is known about the stratus clouds. Age, temperature, and thickness are still basic requirements for precipitation.

Empirical relations between cloud coverage and surface UV have been developed by Ilyas (1987), Bais et al. (1993), and Frederick and Steele (1995). Differences in the derived empirical relationships demonstrate a variation in regional cloud characteristics. All of these factors combine to create strong UV variabilities at the surface, thus complicating detection of long-term trends (Madronich et al., 1998). Therefore, clear cloudless days are best when attempting to correlate the effects of UV with air pollution.

11.1.1.4 Atmospheric Density

As previously stated, the path length of the stratosphere is much longer than that of the troposphere, but the higher density of the troposphere and its increasing scattering capabilities are believed to enhance the absorptive powers of this region (Bruhl and Crutzen, 1989). Atmospheric pressure increases dramatically toward the earth's surface and as a result, the mean free path for molecular interaction is greatly reduced from its value in the stratosphere. From 40 km (the approximate center of the stratosphere) to sea level, the pressure increases almost 1,000 times, and the mean free path changes by at least a factor of 10^6. This, combined with the pollution "soup" that is present in the troposphere and especially concentrated in the planetary boundary layer (PBL), make for an interesting array of interaction cases for each UV photon impacting this portion of the atmosphere.

The planetary boundary layer is approximately 1 km thick and extends from the surface to roughly that height. During the morning hours, it can be as small as 400 m – 800 m and can rise to 1,500 m – 2,000 m during the afternoon with the heating of the layer. This area contains the most significant concentration of air pollutants, especially, aerosols. Land use and surface topography can also cause the PBL to have spatial variations in the layer depth and structure. The spatial variations can also be caused by large-scale meteorological variables. Thermal inversions can compress the PBL, and low pressure systems may increase its thickness.

11.1.1.5 Air Pollution (Gases and Aerosols)

Wide varieties of pollutants are emitted to the atmosphere each year by the tons. The Environmental Protection Agency (EPA) has chosen to classify them in two broad categories based on their respective origination points.

1. Primary Pollutants are those classified as being emitted directly from sources and not undergoing any chemical or physical transformation. An example would be the carbon monoxide emitted through the automobile exhaust. Such gases are called non-reactive since they generally do not interact with other gases nor are they altered by solar radiation.

2. Secondary Pollutants are those that are formed in the atmosphere as a result of chemical reactions among primary pollutants and other species, including radiation that may be present in the atmosphere. One of the most notable of these chemiluminescent reactions is that which leads to the formation of tropospheric ozone. Other reactions can lead to the formations of particulate matter (nitrates,

sulfates), acidic droplets, salt particles, and hydrocarbons.

Pollutants can also be broken into two other categories according to their physical properties: (1) gases such as carbon monoxide (CO), O_3, or SO_2, and (2) particulate matter, such as sulfates, nitrates, black carbon, and the heavier hydrocarbons. Particulates, also commonly known as aerosols, include both solid and liquid particles that become airborne. This includes solids that accumulate water and become difficult to assign optical properties to, as will be shown later. Some of the more common air pollution sources are shown below in Table 11.1.

Table 11.1 Sources of air pollution

Anthropogenic			Natural	
Activity	Source	Pollutant	Source/Activity	Pollutant
Transportation	Autos, buses	CO, NO_x, PM *	Erosion	Windblown PM
Industrial	Mining, pulp and paper mills	PM, H_2S, CO_2	Decay	NH_3, methane, H_2S
Construction	Paving, painting	VOCs **	Forest fires	PM, VOCs, NO_x, etc
Open burning	Leaves, Slash burning, fireplaces, etc.	VOCs, particulate matter	Soil processes	N_2O, CO_2, NH_3
Waste	Household waste disposal	CO_2, methane, H_2S	Evaporation	Sea salts
Power generation	Coal and oil fired plants	Hg, PM hydrocarbons,	Volcanoes	SO_2, CO, Fine PM
			Biogenic emissions	VOC's, terpenes, isoprenes, pollen

* PM = Particulate Matter

** VOCs = Volatile organic compounds

3. Gases. In this chapter it will be proposed that due to the short path length of the UV through the polluted portion of the atmosphere and the normally very low concentrations (parts per billion, ppb) of the gaseous pollutants, there will be little to no effect of these gases on the UV reaching the surface. The dry atmosphere is primarily composed of nitrogen (N_2), O_2, and several inert noble gases—argon (Ar), neon (Ne), krypton (Kr), and xenon (Xe). Their relative concentrations have remained essentially fixed over time (Arya, 1999). The concentrations of water vapor (H_2O) are observed to be highly variable, both in time and space. It is one of the most important ingredients of weather and climate in the lower atmosphere, but is not normally considered an air pollutant. Carbon dioxide (CO_2) also has a relatively high concentration, mostly due to emissions as part of the natural carbon cycle. However, the increasing ambient levels of CO_2, at the current rate of 0.5% per year, are clearly due to anthropogenic emissions from fossil fuel burning, slash burning, and deforestation. Even though increasing levels of CO_2 might be beneficial to agriculture and forestry, as some studies have suggested

(Booker, et al., 2007), the potential consequences of climate warming due to increasing levels of CO_2, methane (CH_4), and other greenhouse gases are considered serious enough to put these gases under the category of air pollutants. Most of the other species that are considered to be air pollutants have both natural as well as anthropogenic sources. Their concentrations in polluted atmospheres, such as over large urban and industrial complexes, are found to be several orders of magnitude higher than the "clean" atmospheric values normally measured in the parts per billion (ppb) range.

Tropospheric ozone has seasonal variations that depend on the sun's intensity, and most importantly, on the strength of the UV radiation. In this case, the UV, in conjunction with oxides of nitrogen and varying types of hydrocarbons, produces the tropospheric ozone. This ozone, in turn, absorbs one of its own creators; the UV radiation. Without the UV, there would be no ozone. Anthropogenic precursors, photochemically reacting in the troposphere, result in accumulations of tropospheric ozone in urban and industrialized regions. These reactions give rise to a diurnal ozone pattern in the more urban regions (Fig. 11.3). Tropospheric ozone is produced in more rural areas by naturally emitted precursors. It can also be transported from nearby urban areas.

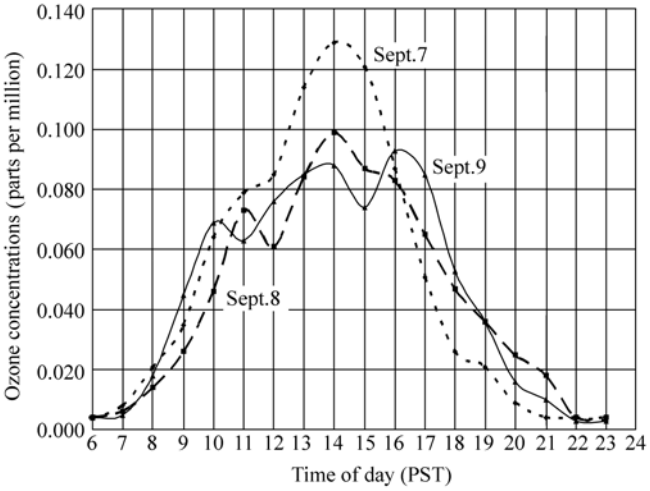

Figure 11.3 Peak ozone concentrations for 3 days in September, Rubidoux, CA

While there are a number of significant gaseous pollutants in the troposphere, only three absorb in the UV region of the spectrum; SO_2, NO_2, and O_3 (Fig. 11.4). As shown in Fig. 11.4, the scattering cross-sections of SO_2 and O_3 are approximately the same magnitude up to about 305 nm, but that of NO_2 is relatively flat in this region and actually surpasses O_3 and SO_2 above 315 nm. Nitrogen dioxide is a precursor for ozone. Its morning peaks can be shown in a daily plot of a polluted urban environment (Fig. 11.5) along with the three peaks of NO_2, UV radiation,

and O_3 (Barnard et al., 2003). As the NO_2 reacts with other pollutants and the incident UV radiation, it produces an afternoon peak of ozone that generally occurs around 14:00 – 16:00 local time. Sulfur dioxide is not a pollutant found during the summer and generally occurs as a result of fossil fuel burning during the winter. Unless found in abnormally high concentrations (greater than 150 parts per billion), the contribution of SO_2 and NO_2 to UV absorption is minimal (less than 1%).

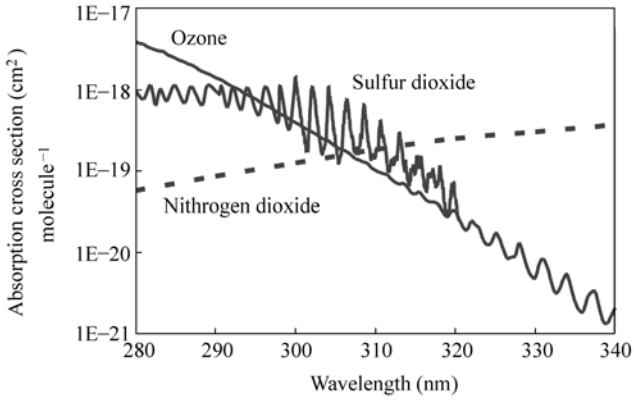

Figure 11.4 Pollutant absorption cross-sections in the UV

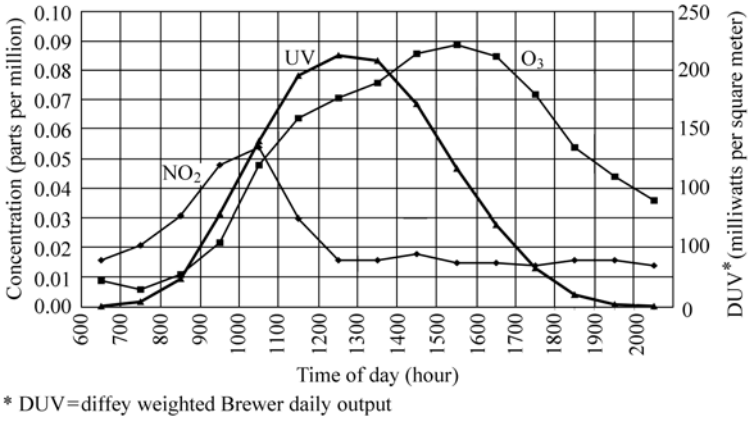

Figure 11.5 Pollution and UV radiation peaks for July 8, 1997. Rubidoux, CA

4. Aerosols. Atmospheric aerosol concentrations provide a complex medium for light scattering and absorption (Ball and Robinson, 1982; Coakley et al., 1983; Charlson et al., 1991; Penner et al., 1992). Coming in all sizes, shapes, hydroscopic, hygroscopic, reflective, refractive, and absorbent, these aerosols create the mathematical soup (mixed and/or layered) through which the UV must pass to get to the earth's surface. They are also present at many altitudes. Volcanic eruptions, such as El Chichon in 1984 and Mt. Pinatubo in 1991, have sent significant

amounts of material into the stratosphere (Stephens, 1995). These materials have reacted with, and depleted the stratospheric ozone. Volcanic gases have reacted at these altitudes to provide fine sulfate particulate matter that is highly reflective. Volcanic materials, gaseous and particulate, have provided the opportunity to assess the climate forcing (Hansen et al., 1997; Kiehl et al., 2000) of stratospheric aerosols (Lacis et al., 1992; Dutton et al., 1994).

Tropospheric aerosol concentrations have increased dramatically since the early 20th century. Anthropogenic emissions have led to increased concentrations over urban areas and have had a significant impact on the air quality east of the Mississippi River valley. Since aerosols have become both positively and negatively implicated in the area of climate change, studies have focused on their radiative properties in the visible and the infrared, but not significantly in the UV region (Flowers et al., 1969). Recently, UV measurements and one of aerosol's main constituents, black carbon (Im et al., 2001), have been implicated in the climate change arena in the southeastern part of the U.S. (Saxena and Menon, 1999). Visible range studies in the eastern United States (Liu et al., 1991) show that biologically active UV reaching the surface has decreased 5%−18% since the industrial revolution. Similar evidence of decreased surface UV-B irradiances attributable to aerosol attenuation has been reported by Seckmeyer and McKenzie (1992), Varotsos et al. (1995), Blumthaler et al. (1996), Mims (1996), and Estupinan et al. (1996). A 14% increase in attenuation of total UV-B irradiance was observed by Lorente et al. (1994), between the highest and lowest turbidity conditions over an urban site. Also observed was an important 27% enhancement of the diffuse UV-B component. For high sun conditions, approximately 50% of UV irradiance was diffuse, and a higher percentage with increasing zenith angle and turbidity. Diffuse radiation, especially for specific species, is very damaging. Frogs laying eggs in what was once thought to be a visibly shady area is now radiated with increased levels of UV, caused by increased aerosols creating a higher percentage of diffuse UV radiation (Blaustein and Wake, 1995; Mims, 1995). The effect of atmospheric aerosols on UV radiation is very complex. It would appear that as opposed to the known adverse effects, increased anthropogenic aerosols have an apparent beneficial effect of reducing surface UV radiation levels, particularly in the presence of increased tropospheric ozone (Bruhl and Crutzen, 1989; Liu et al., 1991).

Black carbon makes up a portion of the aerosol conglomerate in the atmosphere. Concentrations of black carbon in urban areas range up to 13.3 $\mu g/m^3$ (Wolff, 1981), while in the rural areas of western North Carolina, levels can be found in the 0.03 $\mu g/m^3$ range (Bahrmann and Saxena, 1998). It is created in almost all combustion processes, and since it is not degraded under normal atmospheric conditions, wet and dry depositions are its major sinks. Since it occurs primarily in submicron particles (Cadle and Mulawa, 1990), its life in the atmosphere varies from several days to several weeks. It plays an important role in the visibility of the atmosphere through its light extinction properties (Gundel et al., 1984; Cadle

and Mulawa, 1990; Hansen and Rosen, 1990) as well as having catalytic properties that play a role in atmospheric chemistry (Goldberg, 1985). Automotive and diesel exhausts are the prime sources of black carbon.

Particles can also be hydroscopic (absorb water easily) and grow in size. These types frequently reflect radiation due to their outer shell of water, but may also absorb to reradiate at a longer wavelength. Nitrates and sulfates grow from gases in the atmosphere and generally become very good scatterers. Due to the nature of the particle sizes and their ability to retain water, scattering and absorption of light is very wavelength dependent.

11.2 Optics of the Atmosphere

Knowledge of the atmosphere's optical properties is important for radiative transfer modeling studies, remote sensing applications, and climatological studies. In the past, these properties have primarily been studied in the visible and the infrared. Now more attention is being paid to the UV portion to thoroughly understand radiative transfer models. Optical properties of the atmosphere include scattering, emission, and absorption characteristics, which have a strong dependence on wavelength (Reuder and Schwander, 1999). These three processes influence the radiation field in the atmosphere and they each need to be physically and mathematically understood.

11.2.1 Scattering

As one would guess, this denotes a change in the direction in which radiation propagates. Radiation is shifted out of one direction and into another. In general, there can be a shift in frequency upon scattering as well. The wavelength dependence of molecular scattering (i.e., Rayleigh scattering) is proportional to λ^{-4}, so this scattering will be more significant in the UV range than in the visible. The change in direction of radiation associated with scattering is described by the phase function $P(\theta, \phi; \theta', \phi')$ which is dependent upon the size of the particle relative to the wavelength of interest. The phase function describes the probability that an incident photon with incident coordinates (θ', ϕ') is scattered into the direction (θ, ϕ). For molecular scattering the phase function is:

$$P(\Theta) = \frac{3}{4}\left(1 + \cos^2 \Theta\right) \tag{11.1}$$

where Θ is $(\theta - \theta')$. Scattering by larger particles is more complex (Mie scattering), but is generally peaked in the forward direction. This would mean that the left lobe in Fig. 11.6 would be smaller than the right lobe.

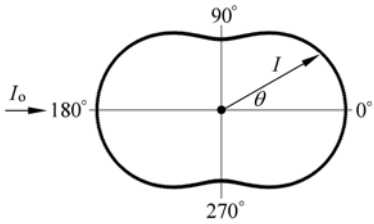

Figure 11.6 Aerosol scattering pattern: Symmetric forward and backward components

Within this category, there are three sub-categories:

1. Rayleigh scattering This type of scattering occurs when the molecules/particles in the atmosphere are smaller than the incident light's wavelength. An example is the blue sky.

Individual air molecules are much smaller than cloud droplets; their diameters are small even when compared with the wavelength of visible light. Each air molecule of O_2 and N_2 selectively scatters the shorter waves of visible light much more effectively than longer wavelengths. As sunlight enters the atmosphere, the shorter visible wavelengths of violet, blue, and green are scattered more effectively by atmospheric gases than are the longer wavelengths of yellow, orange, and especially red. (Violet light is scattered about 16 times more than red light ($\sim 1/\lambda^4$)). As we view the sky, the scattered waves of violet, blue, and green strike the eye from all directions. Since our eyes are more sensitive to blue light, viewing these wavelengths together produces the sensation of blue throughout the sky.

2. Mie Scattering This occurs when the particles are equal to, or larger than, the incident wavelength. In the ambient air pollution realm, there is a peak in the aerosol size distribution near the 2 μm − 3 μm range. Thus, particles in this range would have corresponding Mie scattering wavelengths in the near infrared portion of the spectrum.

Associated with Mie scattering is Mie theory, a system by which electromagnetic wave theory equations are solved using the boundary conditions at the surface of the particle as it interacts with the incoming radiation. It is typically used in a limited realm of spherical particles. By solving the wave equations it is possible to determine the scattered and absorbed electric field around a particle and ascribe an index of refraction to it. This index, being a solution to the wave equation, will have real and imaginary components and characterize the physical properties of the particle. The total solution will also exhibit some phase functions for the scattered field around the particle. These solutions include Bessel and Hankel functions and are beyond the scope of this chapter. Details of these solutions can be found in 'Atmospheric Radiative Transfer' by J. Lenoble (1993).

3. Geometrical scattering This happens when the particulate mater in the air is much larger than the incident wavelength. Rain drops and dust particles fall into this classification.

As a particle increases in size, it scatters light more efficiently. When it reaches

a size that is close to the wavelength of the incident light, it scatters more light than a particle five times its size. These particles remove twice the amount of light intercepted by its geometric cross-sectional area. The laws of geometrical optics may be used to compute the angular distribution of light, which is scattered when a plane electromagnetic wave is incident on a particle much larger than the wavelength of the incident light. Processes involving geometrical optics include rays externally reflected by the particle and rays refracted into the particle; the latter rays may be absorbed in the particle, or they may emerge from it after possibly suffering several internal reflections.

Particles much larger than the incident wavelength also scatter light by means of diffraction, which removes energy from the light wave passing by the particle. The diffraction is concentrated in a narrow lobe around the forward direction, and like geometrical reflection and refraction, it contains an amount of energy equal to that incident on the cross section of the particle. In the far field, the diffracted component of the scattered light may be approximated by the Fraunhofer diffraction theory. The diffraction pattern depends only upon the shape of the cross section of the particle.

We use the term 'ray optics' to describe geometrical reflection and refraction, plus Fraunhofer diffraction. Figure 11.7 illustrates the geometrical configuration for different contributions to light scattered by a large sphere. When hit by radiation, particles can absorb it completely, absorb and reradiate it at a lower, longer wavelength, or completely reflect it. It will generally be a combination of both. The absorption and scattering particle, or molecular cross sections σ_a and σ_s respectively, determine the ability to either absorb or scatter the incoming radiation. Absorption removes photons from the radiation field, whereas scattering changes the photon's direction of propagation. Both functions are particle size/wavelength dependent.

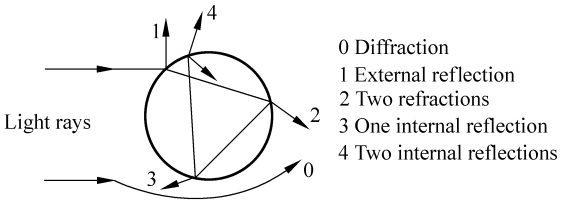

Figure 11.7 Representations of light rays scattered by a sphere according to ray optics, from "An Introduction to Atmospheric Radiation" by K. Liou (1980)

11.2.2 Absorption

Absorption occurs when gas or particulate matter in the air interacts with the UV radiation in such a way as to remove the electromagnetic energy of the UV photon,

and as a result, increases the kinetic energy of the gas or particle. Diesel fuel burning produces a great deal of small black carbon particulate matter. These particles act as very efficient absorbers in the UV region of the spectrum, three times better than in the IR region. This is due to the particle's size (Liousse et al., 1996).

11.2.3 Emission

This is the creation of electromagnetic radiation generally produced as a result of the interactions between the molecules or atoms in the atmosphere with very high energy photons from very short wavelength radiation. These interactions raise either the molecular or atomic state of the gas or particulate matter above its normal ground state and as a result, the gas or particle can emit a longer wavelength of radiation. This emitted radiation is the result of the gas or particle reverting back to its original ground state.

11.2.4 Atmospheric Optical Depth

The optical depth (τ) is the summation of extinction (scattering and absorption) by all the gases and pollutants of the atmosphere:

$$\tau = \int_z^\infty n_j(z)\sigma_j \, \mathrm{d}z \tag{11.2}$$

where n_j is the altitude dependent concentration of the (j) gases and particles that attenuate radiation, each with an effective cross section (scattering and absorption) σ_j. Retrievals of the optical depth from ground-based sensors generally employ two methods: (1) the Langley-plot slope method, and (2) measurements of absolute spectrally-resolved solar flux with a calibrated sun photometer. Each of these methods requires a clear cloudless day to make accurate measurements. The Langley method is a technique based on sun photometry introduced for the first time in November 1725, in France by Pierre Bouguer. This relative measure does not require an absolute calibration of the direct input of the sensor. However, retrievals of optical depths with the Langley method do not provide instantaneous information about the atmospheric optical depth since it requires measurements over a period of time, usually a morning or an afternoon. As a result, it assumes that both total atmospheric optical depth and sensor's sensitivity remain constant during the measurement period. Langley analysis is a linear regression of the natural logarithm (ln) of the signal that is measured vs. air mass (m). A graph of the natural logarithm of the signal vs. air mass falls along a straight line assuming that the atmosphere does not undergo a radical change or the aerosol loading does not change within the measurement time frame. The air mass is defined as

the cosecant of the solar zenith angle for solar angles less than 75°. Above this angle the spherical nature of the atmosphere has to be taken into account, and this involves a more involved calculation (Lenoble, 1993). Extending the straight line to where it crosses the y axis at $m=0$ (zero air mass) yields the extraterrestrial constant, which is the solar flux at the top of the atmosphere. A time averaged extraterrestrial constant is referred to as the characterized Langley intercept for that particular instrument.

Figures 11.8 and 11.9 show two Langley plots derived from Brewer No. 112 during a 1999 summer intensive study at Riverside, California. The data is derived from the PS routine scans taken by the Brewer in the morning and afternoon at 340 nm. The Brewer PS routine looks directly at the sun in the morning and afternoon at various zenith angles to obtain the variables needed to determine the total optical depth. Notice the slight difference in the slopes of the two lines. The slopes are the total optical depths of the atmosphere. The morning slope shows a slightly higher optical depth (OD or ϑ). Since the boundary layer increases with

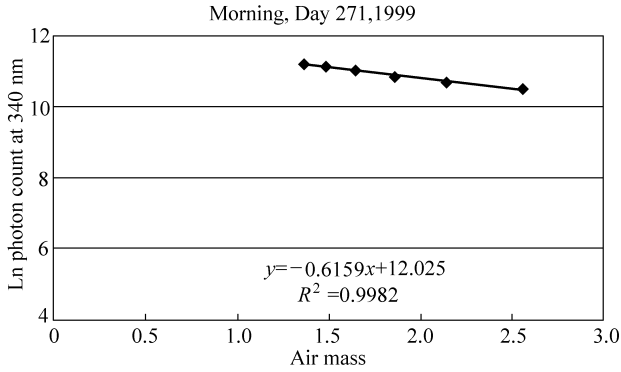

Figure 11.8 Morning Langley plot

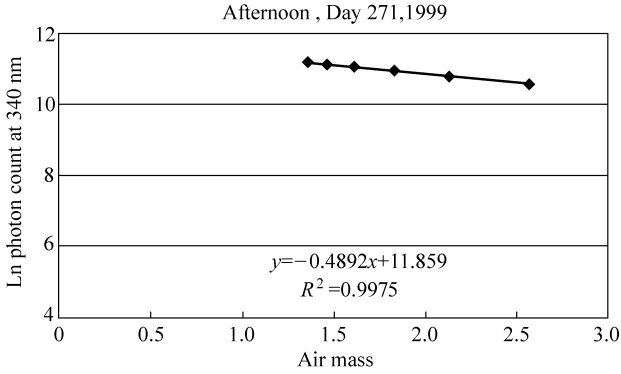

Figure 11.9 Afternoon Langley plot

warming of the atmosphere, the pollutants tend to diffuse as the boundary layer becomes thicker and give a slightly lower OD (ϑ). Other instruments, such as the UV Multi-filter Rotating Shadowband Radiometer (MFRSR), take considerably more data points and can produce Langley plots within an hour or so. This information can be valuable if the atmosphere varies more rapidly than expected.

Measurements taken with a calibrated sun photometer of absolute spectrally-resolved solar flux differ from the standard Langley method in that the extraterrestrial constant is used to directly calculate the total atmospheric optical depth providing instantaneous information about any changes.

Attenuation of a direct solar beam is described by the Beer-Lambert law:

$$I_{\text{dir}} = I_0 \mathrm{e}^{-\tau/\mu_0}$$

I_{dir} is the direct normal irradiance at the surface and I_0 is the extraterrestrial normal irradiance. If this equation is rewritten and applied to the direct solar measurements as taken by the Brewer;

$$\frac{I_\lambda}{I_{0,\lambda}} = -\exp \tau_\lambda m$$

I_λ represents the photon counts measured by the Brewer at wavelength λ and $I_{0,\lambda}$ corresponds to the photon counts that would be measured at the top of the earth's atmosphere. The sum of aerosol and gas extinction is τ_λ and m is the air mass defined as the cosecant of the solar zenith angle. Once the I_0 has been characterized, the total atmospheric optical depth ($\tau_{\text{a},\lambda}$), at a specific wavelength, is calculated using the following:

$$\tau_{\text{a},\lambda} = \left(\frac{1}{m}\right) \ln\left(\frac{I_0}{I_\lambda}\right)$$

I_λ is the Brewer photon count as measured by the PS routine. The natural log of the instrument's photon count (Y-axis) is plotted against the cosecant of the solar zenith angle (X-axis). The slope of the resulting line is the total optical depth.

The total optical depth can be further broken down into its components: (1) the Rayleigh optical depth, (2) the ozone optical depth, and (3) the aerosol optical depth, as shown in Fig. 11.10. One of the objectives for this chapter is to determine the aerosol optical depth (AOD). Anthropogenic aerosols are one of the largest factors affecting surface UV radiation values, but to determine their optical properties is a challenge and one which has many facets. As shown later, the aerosols have a myriad of physical and chemical properties which affect their capabilities to absorb the radiation. Size, chemical composition, and their ability to adsorb or desorb water vapor all contribute to their interaction with the UV.

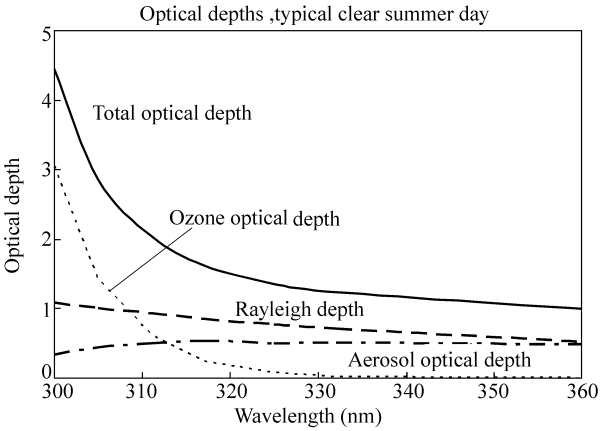

Figure 11.10 The optical depths of the atmosphere

(1) Rayleigh optical depth (Rayleigh scattering): Rayleigh scattering by air molecules is a significant non-pollution contributor to the total optical depth of the atmosphere. It is wavelength dependent, with increased scattering at the shorter UV wavelengths. Rayleigh scattering by the N_2 and O_2 molecules is more significant in the UV portion of the spectra as is shown in the following equation (Dutton et al., 1994).

$$\sigma_{\text{Rayleigh}} = 0.0087 \times \lambda^{-4.05} \times \left(\frac{P_s}{1.013 \times 10^5} \right) \tag{11.3}$$

where λ is wavelength in micrometers and P_s is the atmospheric pressure at the site expressed in Pascals.

(2) Gases: NO_2 and SO_2 also have strong absorption bands in the UV portion of the spectra. The gases can play a small part in determining the total optical depth of the atmosphere, but their concentrations must be extremely high or they must have an extremely long path length. These conditions exist infrequently in the real world. A large SO_2 plume may exist at a soft coal fired power plant or smelter where the concentrations may be very high (much greater than the normal parts per billion normally seen in ambient air). Nitrogen dioxide is normally a by-product of auto emissions, so large concentrations may exist under the right atmospheric conditions (inversions), but even then the path length would be very small, less than a few kilometers.

Total column O_3 is the major absorber of UV radiation due to its relatively large concentration and path length in comparison to other absorbing gases, SO_2 and NO_2. Therefore, measurements of OD obtained from measurements of direct irradiance are directly affected by the total column of O_3 in the atmosphere.

(3) Aerosols: Once the total atmospheric optical depth has been established, the aerosol optical depth (AOD) in the UV is obtained by subtracting the sum of

the Rayleigh and O_3 optical depths. Nitrogen dioxide and SO_2 may contribute to the optical depth in the UV, although their contribution is relatively small (less than 1%). Changes in the total column ozone and the vertical structure of temperature and pressure of the atmosphere have an effect on the retrieved AOD. This effect is small, but non-negligible, in the retrieved AOD for the UV-B ($\lambda < 320$ nm) due to Rayleigh scattering.

Keep in mind though that the UV wavelengths we are talking about generally range between 300 nm and 400 nm. This corresponds to the Rayleigh and the Mie portion of the scattering range described above. Particulate matter found in the atmosphere is generally not found in great quantities below the 1 μ range, but smaller quantities can still be very efficient scatterers.

The selective scattering of blue light by air molecules and very small particles can make distant mountains appear blue, such as the Blue Ridge Mountains of Virginia, North Carolina, and Tennessee. In some remote places, a blue haze may cover the landscape. Hydrocarbon emissions from trees reacting with ozone to produce very small particles selectively scatter blue light and create this haze. When small particles, such as fine dust and salt, become suspended in the atmosphere, the color of the sky begins to change from blue to milky white. Although these particles are small, they are large enough to scatter all wavelengths of visible light fairly evenly in all directions. When our eyes are bombarded by all wavelengths of visible light, the sky appears milky white and when the visibility lowers, we call the day "hazy". If the humidity is high enough, hydroscopic particles will create this haze. Thus, the color of the sky indicates the quantity of the aerosol material suspended in the air. The sky will appear a very deep blue from on top of a very high mountain peak and above the aerosol pollution; a result of Rayleigh scattering.

In a simplified example, for scattering, the luminous flux $=F$, and b is a factor of proportionality; therefore, for a short distance, dl through the atmosphere d$F = -bF$dl. If we integrate both sides we get $F = F_o\, e^{-bl}$. Now if we do the same thing for absorption we get $F = F_o\, e^{-kl}$ where k is another factor of proportionality associated with absorption. If we now combine these two equations, we get $F = F_o e^{-(b+k)l}$ or $F = F_o e^{-\gamma l}$. This last equation is known as the Bouguer/Beer's Law.

Example: In a certain experiment, the luminous flux F is reduced to 36.8% of its original value when a beam of light is passed through an aerosol over a path length of 10 meters. Determine the numerical value of γ in m^{-1}.

From the equation above:

$$F = F_o\, e^{-(b+k)l} = F_o\, e^{-\gamma l} = 0.368$$

$$F/F_o = e^{-\gamma l} = 0.368$$

$$-\gamma l = \ln(0.368) \text{ Since } l = 10 \text{ m}$$

$$-\gamma l = -1.00 \text{ and } \gamma = 0.100 \text{ m}^{-1}$$

These are values that a nephelometer may measure under highly polluted

conditions. A nephelometer measures the ambient light scattering of the atmosphere. This value can be related to the particulate (aerosol) loading of the atmosphere.

11.2.5 Single Scatter Albedo

Absorption and scattering by particles can be simultaneously important, dependent upon the physical-chemical makeup of the particle. The measure of the relative importance of scattering to absorption is the single scatter albedo, ϖ_0, defined as:

$$\varpi_0 = \frac{\sigma_s}{\sigma_s + \sigma_a} \tag{11.4}$$

For purely scattering particles, $\varpi_0 = 1$, and for purely absorbing particles, $\varpi_0 = 0$. Neither extreme will be encountered in the ambient atmosphere where values generally range from 0.55 to 0.95. The single scatter albedo (ω_0) is related to the amount of absorption that is occurring, and is dependent upon particle size, chemical composition, and relative humidity (Kiehl and Rodhe, 1995). Reported values of ω_0 have been primarily restricted to visible and infrared wavelength regions because of the significance to climate change (Hansen et al., 1979; Charlock et al., 1993; Pueschel, 1993). For the UV-B wavelength region, ω_0 is believed to be close to 1.0 for sulfate and marine aerosols and range from 0.5 to 0.7 for desert dust and soot aerosols (Lenoble, 1993; Lacis and Mishchenko, 1995). Madronich (1993) reports a typical ω_0 value at UV wavelengths of 0.8, with a dependence on the levels of chemical impurities in the particles. The amount of moisture available for growth regulates the size of hygroscopic aerosols which in turn affects the scattering efficiency of the aerosol (Charlson et al., 1984). For relative humidities greater than 70%, Waggoner et al. (1981) observed strongly increasing aerosol scattering. When water surrounds an aerosol particle, the particle will not absorb as much, particularly at UV wavelengths since water does not absorb strongly in the UV. Wenny et al. (1998) also found that relative humidity is a controlling factor in the resulting value of ω_0. A larger database encompassing all environmental conditions experienced throughout a year is needed to discern if any seasonal trend exists in ω_0. Based on a short-term study across the Midwest, Ogren and Sheridan (1996) concluded that the dry aerosol ω, for broadband visible radiation is relatively constant in the troposphere both vertically and horizontally, across the U.S. The evidence presented by Wenny et al. (1998) indicates that typically moist climates (such as in the Southeast or Northwest of the U.S) should display larger variations of ω_0 than arid climates (such as in the Midwest and Southwest of the U.S). The magnitude of ω_0 for the dryer atmospheric conditions implies that a fairly substantial portion of aerosol attenuation in the UV is due to absorption. Relative humidities are generally high in the eastern U.S. (typically $> 80\%$), so it is probable that comparatively lower ω_0 values exist in

arid climates and will contribute a significant absorption component to aerosol attenuation of UV-B.

11.2.6 Asymmetry Factor

The asymmetry factor (g) describes the amount of forward or backward scattering by an aerosol particle, and is primarily a function of particle size distribution. The asymmetry factor (g) is a measure of the directionality of scattering, defined as:

$$g = \frac{1}{2}\int_{-1}^{+1} P(\Theta)\cos\Theta \, \mathrm{d}(\cos\Theta) \tag{11.5}$$

and ranges from -1 to $+1$. For symmetric scattering (Rayleigh scattering), $g = 0$. Forward scattering is indicated by $g = +1$ and for backward scattering, $g = -1$. For the UV wavelength region, g typically falls in the range 0.6 to 0.8 (Madronich, 1993). Lacis and Mishchenko (1995) present slight differences in g for aerosols of differing chemical composition. Soot and large desert aerosols generally have $g \approx 0.9$, and for sulfate, marine, and smaller dust aerosols, g ranges from 0.65 to 0.8.

11.2.7 Angstrom's Exponent

Angstrom's formula for spectral extinction has the following form:

$$\tau_a(\lambda) = \beta \times \lambda^{-\alpha} \tag{11.6}$$

where $\tau_a(\lambda)$ is the aerosol optical depth at wavelength λ, β is the extinction at 1 micrometer, α is Angstrom's exponent which is related to the size distribution of the aerosol particles. Cacharro et al. (1989) showed that Angstrom's formula provides a good spectral representation of atmospheric aerosol attenuation. The wavelength to particle diameter ratios is:

- If $\forall = \mathrm{B}\ D/8 << 1$, we will have Rayleigh scattering.
- When particle diameters are between 0.1 and 10 microns we have the case of Mie scattering.
- When $\forall >> 1$, we have the case of geometric optics.

11.3 Models and Measurements

Models can help the researcher determine the UV/pollutant relationships, or the optical properties and physical characteristics of the pollutants utilizing data from numerous sources. Chemical and physical properties can now be retrieved with

regional studies utilizing the newer instrumentation that allows specific ions to be collected and sized. In either case, one must always be aware of the quality of the data that is to be used and must investigate it fully to understand if it will meet the objectives for the accuracy and precision that are being sought. Models are excellent tools for the researcher through which atmospheric optical properties can be determined, but must be tested with real data to insure validity.

Below are two examples of such studies: (1) a statistical study from EPA data banks and a special study carried out by the California Air Resources Board were done to research the pollutant/UV interaction, and (2) an optical properties determination study in which the researchers took their own data from two sites in the mountains of North Carolina. In the second study, the optical properties of various aerosols were researched using models and doing reiterative processes to have the model output coincide with the measured values. Optical properties, such as asymmetry parameter or single scatter albedo, or measured particle sizes and aerosol chemical characteristics, can be determined in this manner. Keep in mind that aerosols are the major contributor to UV absorption in the troposphere and specifically the boundary layer, and ozone is the major absorber of UV in the stratosphere. Additionally, be aware that these studies were done on cloudless days. As mentioned earlier, clouds are major UV absorbers, but their chemical and physical properties and depths are generally not well known.

Study 1:

A study by Barnard (2001) shows that specific air pollutants can reduce the increased surface levels of UV radiation, and offers an explanation for why the expected surface UV increases, caused by decreases in stratospheric ozone, have not been observed, especially in urban regions. Air pollution data (NO_x, O_3, PM-10, SO_2) collected from an EPA UV monitoring site at the University of California at Riverside (UCR), combined with data from a site operated by the California Air Resources Board in Rubidoux, CA, provided the basis of this study. The 1997 South Coast Ozone Study (SCOS) provided three key ingredients: (1) black carbon concentrations, (2) PM-10 concentrations, and (3) collocated radiometric measurements. The Total Ozone Mapping Spectrometer (TOMS) satellite data were used to provide the stratospheric ozone levels that were included in the statistical model. All of these input parameters were used to test this study's hypothesis: "the expected increase of surface UV radiation, caused by decreases in stratospheric ozone, can be masked by increases in anthropogenic emissions." The values for the pollutants were 7:00 a.m. – 5:00 p.m. averages of the instrument's values taken during the summer of 1997. A statistical linear regression model was employed using the stratospheric ozone, black carbon, PM-10, and surface ozone concentrations, and the sin (Θ) and cos (Θ). The angle Θ is defined by: $\Theta = 2\pi$ (Julian date/365). This model obtained a coefficient of determination of 0.94 with an uncertainty level (p-value) of less than 0.3% for all of the variables in the model except ground-based ozone. The final model, regressed against a data set from a

remote, western North Carolina site, resulted in a coefficient of determination of 0.92. The model shows that black carbon can reduce the Diffey weighted UV (DUV) levels that reach the surface by as much as 35%, depending on the season and location.

After review of the various pollutants that absorb in the UV range, only the possibility of PM-10 and a subset of PM-10, the black carbon, and ground-based ozone, were found in high enough concentrations to warrant further investigation. These high concentrations, especially of black carbon, that were found in this urban environment of Riverside-Rubidoux, CA, had not been previously experienced by NC State University personnel who conducted research in the mountains of North Carolina (Im et al., 2001).

Graphs of DUV changes and corresponding stratospheric ozone changes were reviewed for the entire SCOS-97 study. Three days (September 7 – 9), were chosen to study behavioral changes with respect to TOMS ozone, DUV, and black carbon. The graph for this period is shown in Fig. 11.11. Along with the DUV and TOMS, data curves represent the black carbon values for each day of interest. For days 6 – 9, the TOMS ozone value dropped equivalent amounts between days 6 and 7, and between days 8 and 9. However, the DUV increased by over 300 joules m^{-2} from day 6 to day 7, but remained constant from day 8 to day 9, even with a TOMS ozone decrease. In this particular instance, the averaged black carbon for days 6 and 7 is 1.29 μg m^{-3}, while the averaged black carbon for days 8 and 9 is 2.02 μg m^{-3}, a substantial increase. Figure 11.11 also represents the first set of data that are used to relate black carbon and DUV decreases.

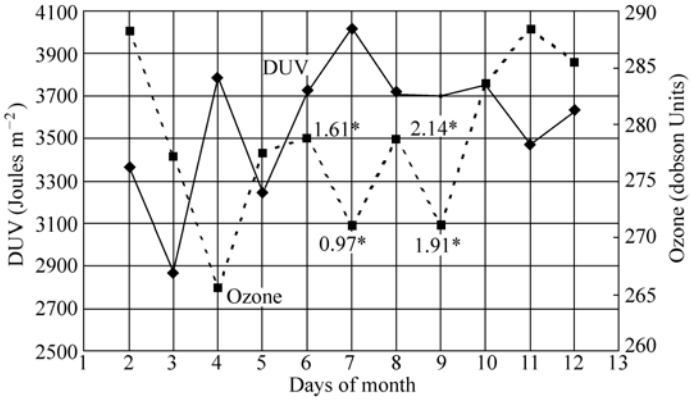

* Numbers on the graph represent black carbon 7:00 a.m. – 5:00 p.m. average in micrograms per cubic meter.

Figure 11.11 Brewer DUV and TOMS Ozone, Sept. 1997

A Statistical Analysis System (SAS) linear regression model was employed that enabled more of the SCOS-97 data to be included. Approximately 63 clear sky days, determined with Brewer DUV readings and the UCR visible data, were investigated.

Ground-based ozone, PM-10, black carbon, and TOMS ozone were used as the independent variables that would be modeled to make up the dependant DUV variable. The model included two other parameters, the sin (Θ) and cos (Θ), to account for DUV seasonal variations caused by the earth's rotation around the sun and the tilt of its axis, where $\Theta = 2\pi$ ((Julian day)$\times(365^{-1})$). Maximum DUV levels at the UC Riverside site occurred during the summer months reaching close to 5,000 joules m^{-2} day^{-1} and minimum levels (781.6 joules m^{-2} day^{-1}) occurred during the winter months.

The results of the SAS linear model are presented below. The final regression developed from this data set is:

$$\begin{aligned}\mathrm{DUV} = {} & 608.91 \sin(\Theta) - 2{,}049\cos(\Theta) - 16.93 \times \mathrm{TOMS} - 7.1 \\ & \times \mathrm{PM\text{-}10} - 148.4 \times \mathrm{Blackcarbon} + 8{,}484. \end{aligned} \tag{11.7}$$

TOMS ozone values are in Dobson units. The units for PM-10 and black carbon are micrograms per cubic meter ($\mu g\ m^{-3}$).

One must be careful at this point in interpreting the results. The *t*-statistics employed here assume a normal distribution, centered on zero with tails in the positive and negative direction. Physically, however, the coefficients for black carbon, PM-10, TOMS, and ground-based ozone must be negative, as all are suspected to be UV radiation absorbers. If positive coefficients had been obtained for any of these independent variables, it would have implied UV radiation had been created, which is not physically possible.

Table 11.2 indicates the sensitivities of each of the parameters used in the model. Table 11.3 was developed using the maxima and minima parameters from this study, and average values based on the author's previous experience in the pollution-monitoring field. The changes noted in Tables 11.2 and 11.3 correlate well with expected physical results. As the Julian day changes from summer (Julian day 180) to winter (Julian day 365), the surface DUV changes dramatically (4,122.3 joules m^{-2}). Likewise, the changes brought about by the TOMS ozone are in line with current literature. A model check done with the radiation amplification factor (RAF) shows excellent agreement with accepted RAF values. This value is known (Madronich et al., 1998) to be between 1.2 and 1.3, and is defined by the percent change in UV divided by the percent change in TOMS ozone. If the change in UV, or in this case DUV, is divided by the mean of the DUV values, a percent change is obtained. Thus, using the appropriate values and the statistical model, the RAF = $16.93 \times 294.5/4{,}036.5 = 1.235$, confirming the relationship between the DUV and TOMS ozone. The surprising factors are the coefficients for the black carbon and the PM-10. Using the values in Table 2, the changes of black carbon and PM-10 encountered in this research account for 46.5% and 58.5%, respectively, of the DUV changes caused by TOMS ozone.

One pollutant, which was not accounted for at all in Eq. (11.1), was the ground-based ozone. Long thought to be one of the significant absorbers of UV-B radiation,

it did not statistically meet the 0.05 significance level in this model. Several trials of the SAS Autoreg procedure, that included non-linear fits of the data and SIN and COS squared terms, did not produce models with coefficients of determination as high as for Eq. (11.1), nor did they produce coefficients that were physically meaningful. When this is carefully analyzed, it makes sense. UV radiation is required to generate the surface measured ozone, but in return, the more ozone, the less UV radiation penetrates to the surface. Also, the more black carbon, the less the UV, and thus the reduction of surface measured ozone.

One factor in the model, which dominates the equation, is the intercept (8,484 joules m^{-2} day^{-1}). This number, much larger than the other terms of the equation, needs some physical explanation. Mathematically, it is the value of the DUV radiation, dependant variable (Y), when all other independent variables (Xs) are zero. Physically it represents a daily averaged DUV value found at the top of the atmosphere. If all the independent variables are removed from the equation, the radiation has no atmospheric constituents to attenuate it and no day-to-day variations caused by the earth's tilting axis and orbit around the sun. If the DUV changes created by these independent variables (Xs) are added to the maximum DUV level from Table 11.2, they sum to 7,994.3 joules m^{-2} day^{-1}. This would approximate a lower boundary level for the daily averaged DUV at the top of the atmosphere. If the same is done for Table 11.3, they sum to 11,481.9 joules m^{-2} day^{-1}. These two numbers represent the range of variations in the DUV values at the top of the atmosphere caused by the maxima and minima values of the factors which alter the radiation as it passes from the top of the atmosphere to the surface. The intercept (8,484 joules m^{-2} day^{-1}) for this model lies within this range. Thus, the intercept could be interpreted as a constant similar to that of the I_0 in the Langley expressions for optical depth.

While this regression was developed utilizing data from a large West Coast experiment in a highly polluted area, it was tested and confirmed in a more pristine, albeit still polluted, East Coast remote site. The Mt. Gibbes site in Mt. Mitchell State Park, NC has been operating for some time with various types of aerosol and radiation equipment. The data from the spring, summer, and fall of 1999 included UV solar radiation and black carbon. TOMS ozone values were obtained from NASA. Since no collocated data were available for the PM-10 concentrations, a yearly averaged value from a neighboring county was used. These were then input into Eq. (11.1) and approximately 30 values of DUV were generated. The values for black carbon at this site ranged from a low of 0.032 μg m^{-3} to a high of 1.545 μg m^{-3}, considerably less than those found at the Riverside site (Table 11.4). UVB-1 data set values, taken at one-minute intervals, were added to obtain a daily (7:00 a.m. – 5:00 p.m.) total UV exposure. This value was then scaled by the CIE (Diffey erythemal curve) factor described in the operations manual for the UVB-1 instrument. The model results were then plotted against these 7:00 a.m. – 5:00 p.m. values.

Table 11.2 Sensitivity tests of DUV in Eq. (11.7) for expected ambient maxima and minima values; the tests consider the parameters of (a) Julian date, (b) TOMS ozone, (c) PM-10, and (d) Black carbon, as the real variables each time, while the others (1999 yearly means) were treated as constants

(a)					
	DUV ($J\ m^{-2}\ d^{-1}$)	Julian Day	TOMS Ozone (DU)	PM-10 ($\mu g\ m^{-3}$)	Black Carbon ($ng\ m^{-3}$)
	777	1			
	3,380	90			
	4,889	180	294	65	1,546
	2,340	270			
	767	365			
Change	4,122				
(b)					
	DUV ($J\ m^{-2}\ d^{-1}$)	TOMS Ozone (DU)	Julian Day	PM-10 ($\mu g\ m^{-3}$)	Black Carbon ($ng\ m^{-3}$)
	3,031	402	183	65	1,546
	5,723	243			
Change	−2,692	159			
(c)					
	DUV ($J\ m^{-2}\ d^{-1}$)	PM-10 ($\mu g\ m^{-3}$)	Julian Day	TOMS Ozone (DU)	Black Carbon ($ng\ m^{-3}$)
	4,164	163	183	294	1,546
	5,271	7			
Change	−1,107	156			
(d)					
	DUV ($J\ m^{-2}\ d^{-1}$)	Black Carbon ($ng\ m^{-3}$)	Julian Day	TOMS Ozone (DU)	PM-10 ($\mu g\ m^{-3}$)
	4,050	7,000	183	294	65
	5,087	10			
Change	−1,037	6,990			

The most striking findings are the results from this testing. As shown in Fig. 11.12, where the modeled data is plotted against the measured UV data from the UVB-1 instrument, there is an excellent correlation, $R^2 = 0.92$. In spite of utilizing one type of instrument to develop the model (Brewer spectrophotometer), and comparing the model's output to that of another type of instrument (Yankee UVB-1), integrated DUV radiation values between the two sites, and the instruments, correlated extremely well. The model (Eq. (11.1)) was applicable for black carbon values ranging from 0.03 $\mu g\ m^{-3}$ to above 4.0 $\mu g\ m^{-3}$, a range of over two decades. It maintained its linearity over this entire range. The Yankee UVB-1 instrument does not have a spectrally resolved output. It measures an entire UV spectrum that includes both the UV-B region and the UV-A region.

Table 11.3 Sensitivity tests for the independent variables of Eq. (11.7) for expected ambient minima and maxima: (a) Julian date, (b) TOMS ozone, (c) PM-10, and (d) Black carbon

(a)					
	DUV	Julian Date	TOMS Ozone	PM-10	Black Carbon
	781.6	0	300 DU	60 μg m^{-3}	1.0 μg m^{-3}
	3,395.3	90			
	4,903.9	180			
	2,355.1	270			
	781.6	365			
Change	4,122.3 joules m^{-2} day^{-1}				
(b)					
	DUV	TOMS Ozone	PM-10	Black Carbon	
	2,364.4	450	60 μg m^{-3}	1.0 μg m^{-3}	
	6,173.6	225			
Change	−3,809.2 joules m^{-2} day^{-1}	225 DU			
(c)					
	DUV	PM-10	TOMS Ozone	Black Carbon	
	3554.9	250	300 DU	1.0 μg m^{-3}	
	5294.4	5			
Change	−1739.5 joules m^{-2} day^{-1}	245 μg m^{-3}			
(d)					
	DUV	Black Carbon	TOMS Ozone	PM-10	
	5,050.8	7.00	300 DU	60 μg m^{-3}	
	4,013.5	0.01			
Change	−1,037.3 joules m^{-2} day^{-1}	6.99 μg m^{-3}			

Table 11.4 Maxima, minima, mean, and standard deviations for the values of the variables used to develop and test the model

	Riverside, CA				Mt. Gibbes, NC			
	Max.	Min.	Mean	Std. Dev.	Max.	Min.	Mean	Std. Dev.
DUV* (J m^{-2} d^{-1})	6,035	2,038	3,698	990	9,677	3,257	6,257	1,764
TOMS (DU)	330	259	285	15	348	270	298	20
PM-10 (μg m^{-3})	132	15	47	20	60**	7	28	12
Black Carbon (ng m^{-3})	4,757	181	1,546	761	1,545	32	395	366
Ozone*** (ppb)	105	25	59	18	na	na	na	na

* UV values obtained from a Brewer spectrophotometer at Riverside, CA and integrated UVB-1 values from Mt. Gibbes, NC.

** PM-10 values from EPA/AIRS database for 1999, yearly average value of 28 used to test model.

*** Ground-based ozone values were used to determine the SAS model, but were not used with the Mt. Gibbes data. Their significance was above the .05 level.

Pollutant concentrations are averages of the hourly averages from 7:00 a.m. – 5:00 p.m.

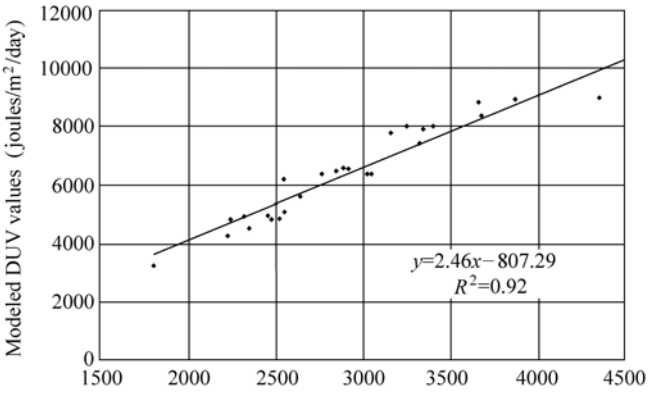

Figure 11.12 UVB-1 Mt. Gibbes daily integrated values

Other studies (Liousse, et al., 1996) have concluded that the black carbon could act to cool the earth, yet UV radiation, being in the shorter end of the spectra, has the highest energy photons. Since the black carbon is absorbing these high-energy photons, and probably re-emitting in the infrared, it would be a logical conclusion that the atmospheric layer in which black carbon resides would be slightly heated. While the UV heating factor would be small, the black carbon absorbs strongly at all wavelengths and can act as a global cooling factor, reducing the available radiation to the earth's surface (Satheesh and Ramanathan, 2000; Yu et al., 2001). The heating of the atmosphere could also impact the photochemical reactions and cloud formations (Ackerman et al., 2000) that occur. There would be a trade-off in this area. The black carbon is reducing the UV that is available to initiate photochemical reactions, but black carbon's presence will also heat the surrounding atmosphere, which tends to speed up these same reactions.

In this particular urban environment, the author found that the black carbon concentrations seem to have little effect on the aerosol optical depth, but did show a relationship with the single scatter albedo. Two papers (Lioussie et al., 1996; Dubovik et al., 1998) that discuss black carbon's optical properties focus on its relationship with the single scatter albedo and not on the optical depth.

In this study statistics and monitoring data led to the formulation of a model that determined an average daily UV dosage at the surface. PM-10 and black carbon were observed to have a significant impact on the UV, but this model still needs to be tested in other regions to refine it with more definitive particulate measurements (chemical composition and size). The research from this study should lead to further investigations that may help develop more quantitative means that would be useful in describing the effects of aerosols on the radiative transfer of UV to the surface. Further work can be done to determine if the long-term increases of automobile and truck emissions are capable of producing the possible effects shown here and to what extent their increases correlate to the decreases of UV radiation. Black carbon's direct and indirect effects on the photochemical

processes in the atmosphere also need to be fully investigated with studies that encompass varied regions.

Study 2:

This study (Wenny et al., 1998) focuses on the attenuation of UV-B that can be attributed to aerosol optical properties. The procedure is to measure UV-B transmission and some aerosol properties in a layer of atmosphere defined by a mountain site and valley site (about 1 km vertically, 6 km horizontally) and analyze the data for aerosol optical effects and aerosol optical properties. The relationship between air mass source region and aerosol optical depth at visible wavelengths and UV-B transmission is investigated. Empirical relations between aerosol optical depth and UV-B transmission are derived to improve predictions of solar noon UV-B transmission, such as done by the U.S. Weather Service (Long et al., 1996). A novel iterative procedure employing Mie scattering and UV-B radiative transfer calculations, in conjunction with actual measurements, is employed to retrieve aerosol optical properties (single scatter albedo (SSA) and asymmetry parameter (AP)) that physically describe the amount of aerosol scattering and absorption occurring, consistent with the observed UV-B transmissions.

The novel approach taken in the present investigation also requires analysis of radiation measurements using Mie theory and radiation transfer calculations; however, the distinction between the present approach and the diffuse/direct method is that the measurement is one of atmospheric irradiance transmission through a layer of atmosphere, determined by the ratio of the irradiance (i.e., diffuse + direct) at the bottom of the layer to the irradiance at the top of the layer, which accurately defines the radiative source illuminating the layer. Moreover, the wavelengths are in the UV region, while the previous investigations were in the visible region.

This study was a step-wise pilot experiment to develop a reliable methodology for gathering an extended set of aerosol information obtained by in situ collections and by confirming the results with measurements and analysis of the radiation field. Long-term measurements are highly desirable for aerosol work because aerosol properties are so variable due to their chemical and spatial inhomogeneous nature; thereby introducing large uncertainties in all radiative and in situ measurement methods of the free atmosphere aerosol.

The aerosol optical depth (τ_λ) was calculated for the three operational wavelength channels of the mountaintop and the valley MFRSR, 415 nm, 500 nm, and 673 nm, using the Langley method. The Langley method assumes that atmospheric attenuation is generally constant throughout the measurement period (airmass length ranging from $m = 2$ to $m = 6$), which is generally true for a clear, stable atmosphere (Lenoble, 1993; Harrison and Michalsky, 1994). Langley plots on all days with clear sky intervals were derived for each instrument's wavelength channels and adjusted to the mean earth-sun distance. Greater variability of the valley instrument was observed and can be attributed to the variability of the atmosphere in the lower layer.

The optical depths for the total column above each respective site, τ_λ, was calculated for each wavelength using an expression of Beer's law

$$\tau_\lambda = -\ln\left(\frac{V_\lambda}{V_{o\lambda}}\right) \times \cos(\theta) \tag{11.8}$$

where τ_λ is the optical depth, V is the instrument output, V_o is the extraterrestrial constant adjusted for earth-sun distance on the day of interest, and θ is the zenith angle. Each τ_λ was calculated as a 12-minute average, centered around the zenith angle of interest.

Wavelength dependent Rayleigh scattering by air molecules was removed from the measurements, as it is a significant non-aerosol contributor to τ_λ. Equation (11.3) was used to estimate the Rayleigh scattering (σ_{Rayleigh}) for each channel. The aerosol optical depth for the layer between the two sites was determined as the subtraction of the Rayleigh-corrected optical depths, $\tau_{\text{valley}} - \tau_{\text{mountain}}$. The absorption optical depth of atmospheric gases, O_3, NO_2, and SO_2 were estimated through calculations using a measured (O_3) or assumed (NO_2, SO_2) column amounts. All three gases were found to have an extremely small contribution to τ_λ, and were thus considered negligible.

The UV-B transmission ($T_{\text{UV-B}}$) for the layer between the two sites was calculated as the ratio of the UV-B measurement at the valley to the UV-B measurement at the mountain. The attenuation of the broadband UV-B irradiance during passage between the sites is assumed to be due to a combination of gaseous and aerosol absorption and scattering.

Aerosol size distributions were measured at the valley site using the Differential Mobility Particle Sizer (DMPS), on nine days coincident with significant clear sky periods. For each of the nine days, an average size distribution was determined from all the distributions collected during the coincident period. Lognormal parameters for the distribution were determined using the fitting software DISTFIT^{TM} provided with the instrument.

A flow chart outlining the method used to derive these aerosol optical properties using a Mie code, similar to the code of Dave (1968), in conjunction with a UV-B radiative transfer code (TUV) (Madronich, 1993) is shown below in Fig. 11.13. The resulting end product is the aerosol optical properties (at UV-B wavelengths) of an atmospheric layer between a mountain valley site and peak site in western North Carolina.

The lognormal parameters derived from the measured aerosol size distributions served as input to the Mie code using a first-guess for the complex index of refraction of $1.5 - 0.08i$ (1.5 is held constant). The Mie code calculations yield first-guess estimates of the asymmetry factor and single scatter albedo at 312 nm, the UVB-1's wavelength of maximum sensitivity to atmospheric UV. These values serve as input into the UV-B radiative transfer model of the UV-B transmission for the spectral response function of the Yankee UVB-1 radiometer. Additional inputs

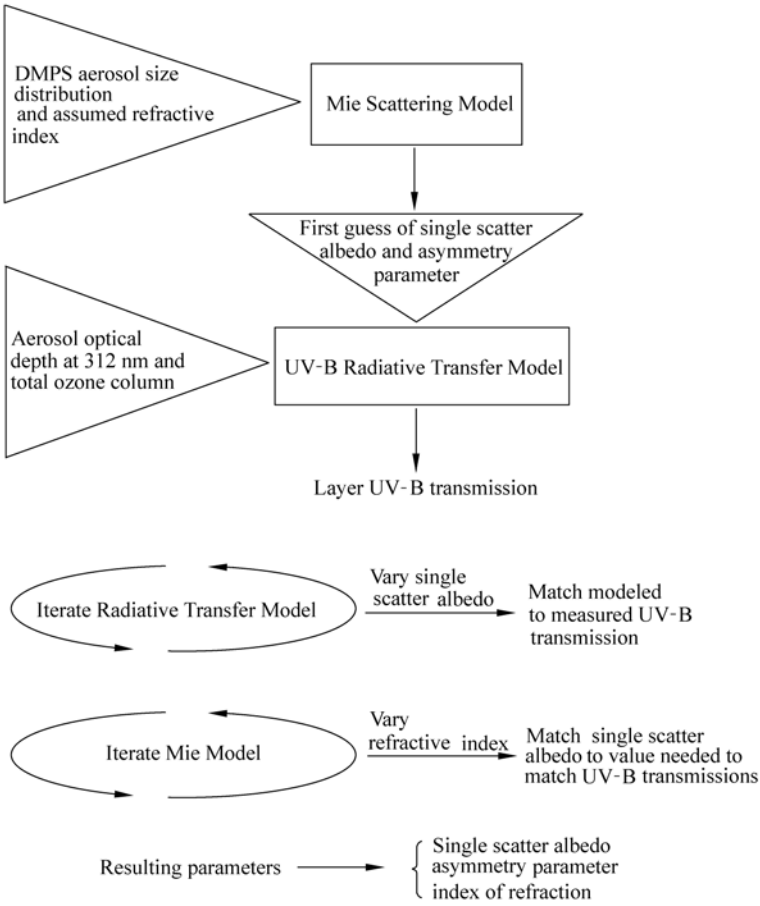

Figure 11.13 Diagram outlining the modeling procedure used to determine single scatter albedo and the asymmetry parameter

are the total ozone column as measured by the valley Brewer spectrophotometer and the aerosol optical depth at 312 nm, extrapolated from the spectral extinction determined from the τ_λ values of the MFRSR. This extrapolation of τ_λ to 312 nm is based on Angstrom's Formula for spectral extinction and has the following form:

$$\tau_a(\lambda) = \beta \times \lambda^{-\alpha} \tag{11.9}$$

where $\tau_a(\lambda)$ is the aerosol optical depth at wavelength λ, β is the turbidity coefficient, α is Angstrom's exponent which is related to the size distribution of the aerosol particles. Cachorro et al. (1989) showed that Angstrom's formula provides a good spectral representation of atmospheric aerosol attenuation. Iteration, varying the single scatter albedo, until the modeled transmission through the layer matched the observed transmission as measured by the UVB-1 instruments and then, varying the imaginary component of the complex index of refraction

until the single scatter albedo matched the value resulting from the radiation code iteration was repeated until convergence was achieved. UV-B transmission is more sensitive to changes in ϖ_0 (compared to g), thus the decision to use it as the varying parameter. The aerosol size distribution acts as a constraint on g, which only changed slightly as the refractive index changed.

Optical depth values were obtained for all clear-sky periods throughout the six month observational period with a mean optical depth for the entire atmosphere as measured from the valley MFRSR at 500 nm of 0.356. The large seasonal variability inherent in optical depth measurements is evident by a standard deviation of 0.329. Past studies of annual turbidity cycles in nearby regions are consistent with this mean value (Flowers et al., 1969).

Clear-sky conditions were present over the two research sites for a large portion of the morning hours on 46 days. Using back trajectory analysis, 18 of these cases were classified as highly polluted air masses, 15 as polluted marine and 13 as polluted continental. Air masses arriving at the site from these sectors have been shown to exhibit differing physio-chemical characteristics (Deininger and Saxena, 1997; Ulman and Saxena, 1997). The MFRSR optical depth measurements for the intervening layer were categorized according to air mass source region. It was found that the τ mean values differed for the three air mass types suggesting that aerosol optical properties vary in relation to air mass. The highest mean value of τ for the highly polluted air mass classification is consistent with an assumption of higher sulfate aerosol concentrations, as this aerosol species has been shown to be an efficient attenuator at visible wavelengths (Whitby, 1978; Hegg et al., 1993; Yuen et al., 1994). The greater standard deviation of the highly polluted air mass cases is indicative of the greater variation in aerosol characteristics arising from differences in source strength, composition, size distribution and age of the aerosol. Two aerosol size distributions (highly polluted classification) displayed a multi-modal shape, which indicates the presence of an accumulation mode (particle diameter between 0.1 μm and 1.0 μm). Assuming that sulfate aerosols are the predominant species in the highly polluted air mass, the presence of a significant accumulation mode is not unexpected and can be explained through condensation and coagulation of sulfate aerosols. The nine clear sky days with DMPS aerosol size distribution measurements permitted a closer examination of the relationship of aerosol and radiative properties using the iterative procedure defined previously.

For the nine days investigated, ϖ_0 at 312 nm varied from 0.75 to 0.93 and showed no discernible dependence on air mass type; however, a dependence on relative humidity was observed. The three days possessing the highest relative humidities have $\varpi_0 > 0.9$, which is consistent with the characteristics of hygroscopic aerosols, which do not absorb strongly in the UV. The remaining six days exhibited ϖ_0 values of 0.75 to 0.82, comparable to the typical value given by Madronich (1993). This relatively narrow range of ϖ_0 for dryer conditions indicates that relative humidity is a controlling factor in the resulting value of ϖ_0.

The small sample size did not allow determination of any seasonal trend in ϖ_0. The evidence from this study indicates that typically moist climates (such as in the Southeast or Northwest U.S.) will display larger variations of ϖ_0 than arid climates (such as in the Midwest and Southwest U.S.). According to our results, the magnitude of ϖ_0 for the dryer atmospheric conditions implies that a fairly substantial portion of aerosol attenuation in the UV is due to absorption. Relative humidities are generally high in the eastern U.S. (typically > 80%), so it is probable that comparatively lower ϖ_0 values exist in arid climates and will contribute a significant absorption component to aerosol attenuation of UV-B. The ϖ_0 values found in this study are in general lower than those used in several UV modeling studies (Liu et al., 1991; Wang and Lenoble, 1994). The nine *g* values determined for our site fall within 0.63 to 0.76. No specific feature based upon air mass is discernible. Angstrom's exponent (α) was determined using the MFRSR spectral aerosol optical depth data and also the volume spectral extinction as calculated by the Mie code. The good agreement for five of the nine cases, evident from the small differences between the two values, gives increased confidence in the modeling procedure results. The larger differences for the remaining four cases can be attributed to greater uncertainty in the aerosol size distribution measurements. The effect of aerosol chemical composition on UV-B transmission is unquantified in this investigation. Future studies should incorporate coupled measurements of aerosol size distribution, aerosol chemical composition characteristics and in-situ aerosol optical properties. Such combined measurements are rarely obtained (Schwartz et al., 1995).

Extrapolation of the spectral extinction curve, determined from $\ln(\tau)$ versus $\ln(\lambda)$ fit with linear regression permits an estimate of τ_{312} for each day. A plot of ln(Solar Noon UV-B Transmission) versus τ_{312} exhibits a strong correlation ($r^2 = 0.904$). The fit is surprisingly good considering the wide range of solar noon zenith angles, 20° to 55°, for the nine days used. The linear regression equation provides a simple expression for determining solar noon UV-B transmission if a value of τ_{312} is known. The regression equation is as follows:

$$\ln(\text{UV-B Transmission at Solar Noon}) = -0.1422 \times (\tau_{312}) - 0.138 \qquad (11.10)$$

The *y*-intercept, i.e. no aerosol attenuation, converts to a transmission of 87.1%.

The average transmission for each clear morning was derived for the UVB-1 measurements. A morning average transmission was determined for the zenith range $65° - 40°$ as the transmission changed by less than 3% over this period for any given day. The highly polluted cases exhibited, on average, the lowest transmission, 77.8% ± 4.6%. The polluted marine cases exhibited an average transmission of 81.9% ± 2.9%, and the polluted continental cases 83.5% ± 2.8%. The observed differences are due both aerosol differences and the abundance of absorbing gases. The mean ozone column for the layer was 12.6 DU (±6 DU), and showed no discernible trend versus air mass type. A change in layer ozone column of 10 DU

resulted in an UV-B transmission change of only 1.5% (decreased transmission for increased ozone and vice versa). The effect of SO_2 and NO_2 absorption on UV-B transmission was modeled and showed a decrease in UV-B transmission of much less than 0.5% for the typically minute layer column amounts of each gas. Differences in gaseous absorption, although small, can account for a portion of the variability between air mass types and also the variability within a given air mass type. Therefore, the remainder of the variability is primarily due to differences in aerosol attenuation properties. Highly polluted air masses, which exhibited the highest aerosol optical depth, also exhibited the greatest attenuation of UV-B. In comparison, the "cleaner" marine and continental air masses had lower average τ_λ values and higher UV-B transmission values. Our observed range of broadband UV-B attenuation for all the days was $14\%-31\%$ for the 1 km layer. This range is quite consistent with the other reported values of an altitude effect, or the percentage decrease per 1,000 meters altitude in the lower troposphere.

An important aspect of this study is the development of an empirical relationship between optical depth and UV-B transmission, useful for calculation of the NOAA UV Index, UV climatology studies, and remote sensing applications. Specific knowledge of aerosol parameters and their effects on UV-B transmission allow for improved accuracy in UV climatology modeling. There is an inherent regionality to optical depth and aerosol optical properties which will in turn cause regional differences in UV-B transmission, and this needs to be considered in such applications as UV forecasts, UV climatology and long term trends. Remote sensing applications that rely upon UV attenuation measurements need to account for any change in aerosol UV attenuation due to changing aerosol properties.

To investigate the effect of aerosols alone, it is necessary to utilize an instrument that measures in wavelength bands where non-aerosol attenuation is minimized, such as the three channels from the MFRSR (415 nm, 500 nm, and 673 nm). Ideally, aerosol optical depths at wavelengths in the UV-B region would yield the best relation. However, optical depths at UV-B wavelengths are more problematic to obtain. Plots of natural logarithm of UV-B transmission versus aerosol optical depth were made for solar zenith angles of 65° to 40° in 2.5° intervals. Individual zenith angle plots were made as opposed to daily averaged plots because global UV-B transmission is slightly dependent upon zenith angle. Each plot was negatively correlated, i.e. increased aerosol optical depth results in decreased UV-B transmission. The correlation coefficient (r^2) values for each plot show that the regressions fit very well, with only 4 of the 33 regressions having an $r^2 < 0.8$. For each wavelength, the slope, or change in ln(UV-B transmission) for a given change in τ, decreases as zenith angle decreases. This implies that as the sun nears solar noon and a shorter atmospheric pathlength, the UV-B transmission becomes less sensitive to τ and also that the UV-B transmission approaches a maximum value. This is of importance in biological terms since the hours surrounding solar noon are the times of maximum irradiance.

For a given zenith angle, the regression slopes increase as the wavelength increases due to the fact that optical depth is proportional to λ^{-1}. The larger range of optical depths at the shorter wavelengths is reflected in a smaller percentage change in UV-B transmission (lesser slope) associated with a given change in aerosol optical depth. Since a given change in aerosol concentration produces a more significant variation in optical depth for shorter wavelengths, the sensitivity of UV-B transmission to aerosol optical depth must be less at these wavelengths. A percentage change in UV-B transmission for a given change in aerosol optical depth can be determined from the regressions. Using the 500 nm plot at 50° solar zenith angle as an example, a change in optical depth of 0.1 predicts a change in the UV-B transmission on the order of 4%. An additional feature of interest is the nearly constant value of the *y*-intercept values. Upon conversion to percent UV-B transmission, the averages of the *y*-intercepts over all zenith angles are $86.8\% \pm 0.7\%$ for the 415 nm channel, $87.0\% \pm 0.8\%$ for the 500 nm channel, and $87.0\% \pm 0.7\%$ for the 673 nm channel. Thus, 87% is the UV-B transmission expected for an aerosol free layer and the 13% attenuation can be ascribed to Rayleigh scattering in addition to the slight absorption by atmospheric gases, i.e., O_3, NO_2, and SO_2, in the layer. This value is consistent with the zero aerosol conditions derived for the nine day case study results discussed previously. Multiple regression analysis using the Statistical Analysis System (SAS) was performed to obtain the full model for prediction of the UV-B transmission versus zenith angle (in degrees) given a set of aerosol optical depth measurements, and the backward elimination procedure was used to identify the most significant variable. Aerosol optical depth at 415 nm (τ_{415}) was determined as the most significant variable for predicting UV-B transmission, with the ability to account for 72.8% of the data variability. Upon including the parameters τ_{500} and zenith angle (the two next most significant parameters) the fit improves to account for 82.0% of the observed variability. All three variables are significant at the 0.0001 level. The empirical regression equation is of the form:

$$\ln(\text{UV-B transmission}) = a_0 + a_1 \times \tau_{415} + a_2 \times \tau_{500} + a_3 \times \text{zenith angle} \qquad (11.11)$$

where the regression coefficients are defined as $a_0 = -0.0935$, $a_1 = -0.8515$, $a_2 = 0.7505$, and $a_3 = -0.0012$. The addition of the two extra terms, resulting in a 10% improvement in fit, was deemed necessary as the inclusion of a zenith angle term enables prediction for UV-B transmission at solar noon, and the use of two optical depth values provides information on the spectral extinction shape. The τ_{673} term was neglected, as inclusion did not significantly improve the quality of the fit (0.1% improvement). The 18% variability unaccounted for can be ascribed to the combined uncertainties of the measurements as well as factors, each individually small, not included in the regression (i.e., variations in ozone, aerosol absorption, chemical composition, and relative humidity). Equation (11.11) is specific to the region surrounding the experiment sites.

11.4 Summary

As previously shown in this chapter, the main constituent of air pollution that affects the transmission of UV to the earth's surface is aerosols. While three gases exhibit strong UV absorption characteristics, their concentrations and path-lengths in the troposphere, and primarily the planetary boundary layer, are both insufficient to produce significantly reduced UV levels at the surface. The physical, chemical and optical properties were studied, and the results strongly indicate that for dryer conditions, the retrieved single scatter albedo was higher in the eastern part of the U.S., and that relative humidity played an important role in determining this level of single scatter albedo. Highly polluted air masses also exhibited larger aerosol optical depths and in turn, the lowest UV transmission.

The second study also showed a novel non-invasive remote sensing procedure. A Mie scattering code and a radiative transfer model were utilized in conjunction with measured parameters to retrieve reasonable values of aerosol single scatter albedo and asymmetry factor using transmission and size distribution measurements. The aerosol single scatter albedo was seen to vary substantially; a probable cause due to the concentrations of black carbon in the atmosphere.

There is an obvious need to initiate an investigation similar to the Wenny study that monitors both the radiation and the aerosol size and speciation at the top of a mountain and in a nearby valley. Recent advances in aerosol instrumentation allow researchers to not only perform real time monitoring of aerosol size distributions, but are also now able to determine aerosol speciation. These data, combined with the procedures presented here, can fully characterize certain aerosol classes within a study area that could be applied throughout the country. Sulfates and nitrates, both thought to be highly scattering media, can each be detected in real time with ion chromatography. An aethalometer can measure black carbon, a DMPS or similar instrument can measure aerosol size distributions, and a good relative humidity or dew point hygrometer, combined with either a Brewer spectroradiometer or a UV MFRSR, should be able to fully characterize the aerosol optical properties in the UV and relate them to the species of aerosols present in the ambient atmosphere.

A recent paper by Petters et al. 2003 describes a methodology that can be used with the UV MFRSR and coupled with a tropospheric UV radiative transfer model to produce values of the single scatter albedo. This study conducted at the same site as the Wenny study has slightly wider variations than previously reported values. The lower values of SSA could indicate that, at least at this site, preferential absorption of UV radiation by black carbon aerosols could be occurring. More SSA data taken in the UV spectrum will allow for better estimation of this parameter for UV radiative transfer modeling and will lessen the modeling error in determining surface UV irradiances.

All of a study's monitoring data must have its quality control factors of precision, accuracy, representativeness, completeness, and comparability known

and documented prior to the beginning of the study. If EPA data are used, the state of the local agency that reports that data to EPA will have a complete set of such documents that will include a Quality Systems Implementation Plan and a systematic approach to provide external system and performance audits. The data quality must be maintained throughout the study. It is a waste of the investigator's time, and more importantly, money, to gather data that cannot be used, simply because its accuracy and precision were not documented. This is true for both the air pollution data and the radiation data.

One must keep in mind that there have only been two studies presented here to show the methodology employed in determining site specific UV transmissions to the surface. Each site will have its own variables, not the least of which will be the differing combinations of scattering and absorbing aerosols. There is a great need to characterize more sites and identify aerosol types according to their chemical species and by doing so, relate the species to the single scatter albedo and the aerosol optical depth. By doing this it will become possible to transfer the ground-based knowledge to satellite observation points so that predictions of surface UV can become a reality.

The reader is referred to the Indian Ocean Experiment (INDOEX), a 1999 international field campaign conducted to study how air pollution affects climate processes over the tropical Indian Ocean, and to the South Coast Ozone Study (SCOS'97) conducted in the Los Angeles Basin during the summer of 1997 where radiation and pollution measurements were taken at the surface and various altitudes. Numerous publications were produced from each of these studies.

References

Ackerman AS, Toon OB, Stevens DE, Heymsfield AJ, Ramanathan V, and Welton EJ (2000) Reduction of Tropical Cloudiness by Soot. Science 288: 1042 – 1047

Arya SP (1999) Air Pollution Meteorology and Dispersion. Oxford University Press, New York, p.301

Bahrmann CP, and Saxena VK (1998) The influence of air mass history on black carbon concentrations in the southeastern US. J. Geophys. Res. 103: 23153 – 23161

Bais AF, Zerefos CS, Meleti C, and Ziomas IC (1993) Spectral measurements of solar UVB radiation and its relation to total ozone, SO_2, and clouds. J. Geophys. Res. 98: 5199 – 5208

Ball RJ, and Robinson GP (1982) The origin of haze in the central United States and its effect on solar radiation. J. Appl. Meteorol. 21: 171 – 188

Barnard WF (2001) Daily Surface UV Exposure and Its Relationship to Surface Pollutant Measurements. PhD. Thesis

Barnard WF, Saxena VK, Wenny BN, and DeLuisi JJ (2003) Daily surface UV exposure and its relationship to surface pollutant measurements, Journal of the Air & Waste Management Association, Vol 53

Blaustein AR, and Wake DB (1995) The puzzle of declining amphibian populations. Scientific American 52 – 57

Blumthaler M, Schreder J, and Grobner J (1996) UV sky radiance influenced by aerosols and tropospheric ozone-measurements and modeling. In: Smith WL, Stamnes K (eds) IRS '96: Current Problems in Atmospheric Radiation. Proc. Int. Radiation Symp., Fairbanks, AK, Deepak Publishing, Hampton, VA, pp.853 – 856

Bojkov RD, Fioletov VE, and Diaz SB (1995) The relationship between solar UV irradiance and total ozone from observations over southern Argentina. Geophysics Research Letters 22: 1249 – 1252

Booker FL, Burkey KO, and Pursley WA (2007) Elevated carbon dioxide and ozone effects in peanut. I. Gas-exchange, biomass, and leaf chemistry. Crop Science 47: 1475 – 1487

Bruhl C, and Crutzen PJ (1989) On the disproportionate role of tropospheric ozone as a filter against solar UV-B radiation. Geophys. Res. Lett. 16: 703 – 706

Cachorro VE, Gonzalez MJ, De Frutos AM, and Casanova JL (1989) Fitting Angstrom's formula to spectrally resolved aerosol optical thickness. Atmos. Environ. 23: 265 – 270

Cadle SH, and Mulawa PA (1990) Atmospheric carbonaceous species measurement methods comparison study: general motors results. Aerosol Science Technology 12: 128 – 141

Charlock TP, Kondratyev K, and Prokofyev M (1993) Review of recent research on the climatic effect of aerosols. In: Jennings SG (ed) Aerosol Effects on Climate, Univ. of Arizona, Tucson, pp.233 – 274

Charlson, RJ, Covert DS, and Larson TV (1984) Observation of the effect of humidity on light scattering by aerosols. In: Ruhnke L, Deepak A (eds) Hygroscopic Aerosols. Deepak Publishing, Hampton, VA

Charlson RJ, Langner J, Rodhe H, Leovy CB, and Warren SG (1991) Perturbation of the Northern Hemispheric radiative balance by backscattering from anthropogenic sulfate aerosols. Tellus 43B: 152 – 163

Coakley JA, Jr, Cess RD, and Yurevich FB (1983) The effect of tropospheric aerosols on the earth's radiation budget: A parameterization for climate models. J. Atmos. Sci. 40: 116 – 138

Dave JV (1968) Subroutines for computing the parameters of electromagnetic radiation scattered by a sphere. IBM Scientific Center, Palo Alto, CA, Rep. No. 320 – 3237

Deininger CK, and Saxena VK (1997) A validation of back trajectories of air masses by principal component analysis of ion concentrations in cloud water. Atmos. Environ. 30: 295 – 300

Dubovik O, Holben BN, Kaufman YJ, Yamasoe M, Smirnov A, Tanre D, and Slutsker I (1998) Single-scattering albedo of smoke retrieved from the sky radiance and solar transmittance measured from the ground. J. Geophys. Res. 103: 31903 – 31923

Dutton EG, Reddy P, Ryan S, and DeLuisi JJ (1994) Features and effects of aerosol optical depth observed at Mauna Loa, Hawaii: 1982 – 1992. J. Geophys. Res. 99: 8295 – 8306

Estupinan JG, Raman S, Crescenti GH, Streicher JJ, and Barnard WF (1996) Effects of clouds and haze on UV-B radiation. J. Geophys. Res. 101: 16807 – 16816

Fioletov VE, and Evans WFJ (1997) The influence of ozone and other factors on surface radiation Ozone Science: a Canadian Perspective on the Changing Ozone Layer. University of Toronto Press, Toronto, pp.73 – 90

Flowers EC, McCormick RA, and Kurfis KR (1969) Atmospheric turbidity over the United States, 1961 – 1966. J. Appl. Meteor. 8: 955 – 962

Frederick JE, Koob EK, Alberts AD, and Weatherhead EC (1993) Empirical studies of tropospheric transmission in the ultraviolet: broadband measurements. J. Appl. Meteor. 32: 1883 – 1892

Frederick JE, and Steele HD (1995) The transmission of sunlight through cloudy skies: an analysis based on standard meteorological information. J. Appl. Meteorol. 34: 2755 – 2761

Goldberg ED (1985) Black carbon in the environment: Properties and distribution. Wiley Interscience

Gundel LA, Dod RL, Rosen H, and Novakov T (1984) The relationship between optical attenuation and black carbon concentration for ambient and source particles. Science Total Environment 36: 197 – 202

Hansen ADA, and Rosen H (1990) Individual measurements of the emission factor of aerosol black carbon in automobile plumes. Journal of Air Waste Management Association 40: 1654 – 1657

Hansen JE, Lacis AA, Lee P, and Lang WC (1979) Climatic effects of atmospheric aerosols. In: Proc. Conf. on Aerosols: Urban and rural characteristics, source and transport studies, 1977. New York Academy of Sciences, pp.575 – 587

Hansen J, Sato M, Lacis A, and Ruedy R (1997) The missing climate forcing. Philosophical Transactions of the Royal Society of London Series B-Biological Sciences 352: 231 – 240

Harrison L, and Michalsky J (1994) Objective algorithms for the retrieval of optical depths from ground-based measurements. Appl. Opt. 33: 5126 – 5132

Hegg DA, Ferek RJ, and Hobbs PV (1993) Light scattering and cloud condensation nucleus activity of sulfate aerosol measured over the Northeast Atlantic Ocean. J. Geophys. Res. 98: 14887 – 14894

Ilyas M (1987) Effect of cloudiness on solar ultraviolet radiation reaching the surface. Atmos. Environ. 21: 1483 – 1484

Im J-S, Saxena VK, and Wenny BN (2001) Temporal trends of black carbon concentrations and regional climate forcing in the southeastern United States. Atmospheric Environment 35: 3293 – 3302

Kerr JB, and McElroy CT (1993) Evidence for large upward trends of ultraviolet-B radiation linked to ozone depletion. Science 262: 1032 – 1034

Kiehl JT, and Rodhe H (1995) Modeling geographical and seasonal forcing due to aerosols. In: Charlson RJ, Heintzenberg J (eds) Aerosol Forcing of Climate. John Wiley & Sons, Chichester, U.K.

Kiehl JT, Schneider TL, Rasch PJ, Barth MC, and Wong J (2000) Radiative forcing due to sulfate aerosols from simulations with the National Center for Atmospheric Research, Community Climate Model, Version 3. J. Geophys. Res.-Atmos. 105: 1441 – 1457

Lacis A, Hansen J, and Sato M (1992) Climate forcing by stratospheric aerosols. Geophys. Res. Lett. 19: 1607 – 1610

Lacis AA, and Mishchenko MI (1995) Climate forcing, cloud sensitivity, and climate response: a radiative modeling perspective on atmospheric aerosols. In: Charlson RJ, Heintzenberg J (eds) Aerosol Forcing of Climate. John Wiley & Sons, Chichester, U.K.

Lenoble J (1993) Atmospheric Radiative Transfer. A Deepak Publishing, Hampton, VA, p.532

Liou K (1980) An introduction to atmospheric radiation Kuo-Nanliou. An International Geophysics Series. Volume 26, Academic Press, San Diego, CA, p.392

Liousse C, Penner JE, Chuang C, Walton JJ, Eddleman H, and Cachier H (1996) A global three-dimensional model study of carbonaceous aerosols. J. Geophys. Res. 101: 19411 – 19432

Liu SC, McKeen SA, and Madronich S (1991) Effect of anthropogenic aerosols on biologically active ultraviolet radiation. Geophys. Res. Lett. 18: 2265 – 2268

Long CS, Miller AJ, Lee H-T, Wild JD, Przywarty RC, and Hufford D (1996) Ultraviolet index forecasts issued by the National Weather Service. Bull. Am. Meteorol. Soc. 77: 729 – 748

Lorente, J, Redano A, and DeCabo X (1994) Influence of urban aerosol on spectral solar irradiance. J. Appl. Meteor. 33: 406 – 415

Ma J, and Guicherit R (1997) Effects of stratospheric ozone depletion and tropospheric pollution on UVB radiation in the troposphere. J. Photochem. Photobio. 66: 346 – 355

Madronich S (1993) The atmosphere and UV-B radiation at ground level. In: Young AR (ed) Environmental UV Photobiology. Plenum Press, New York

Madronich S, McKensie RL, Bjorn LO, and Caldwell MM (1998) Changes in biologically active ultraviolet radiation reaching the earth's surface. J. Photochem. Photobio. B46: 5 – 19

McKenzie RL, Matthews WA, and Johnson PV (1991) The relationship between erythemal UV and ozone, derived from spectral irradiance measurements. Geophys. Res. Lett. 18: 2269 – 2272

Mims FM (1995) Vanishing Frogs. Scientific American 273: 10

Mims FM (1996) Biological effects of diminished UV and visible sunlight caused by severe air pollution. In: Smith WL, Stamnes K (eds) IRS '96: Current Problems in Atmospheric Radiation. Proc. Int. Radiation Symp., Fairbanks, AK, 19-24 August, 1996, Deepak Publishing, Hampton, VA, pp.905 – 908

Mims FM, Barnard WF, Neuendorffer AC, and Labow GJ (1995) Unusually Low Ozone Detected Over South-Central U.S. EOS 76: 113 – 115

Ogren, JA, and Sheriden PJ (1996) Vertical and horizontal variability of aerosol single scattering albedo and hemispheric backscatter fraction over the United States. In: Proceedings of the 14th International Conference on Nucleation and Atmospheric Aerosols, Helsinki, Finland

Penner JE, Dickinson RE, and O'Neill CA (1992) Effects of aerosol from biomass burning on the global radiation budget. Science 256: 1432 – 1434

Petters JL, Saxena VK, Slusser JR, Wenny BN, and Madronich S (2003) Aerosol single scattering albedo retrieved from measurements of surface UV irradiance and a radiative transfer model. J. Geophys. Res. 108(D9):4288, doi:10.1029/2002JD002360

Pueschel RF (1993) Potential climatic effects of anthropogenic aerosols. In: Jennings SG (ed) Aerosol Effects on Climate. Univ. of Arizona, Tucson, 110 – 132

Reuder J, and Schwander H (1999) Aerosol effects on UV radiation in non-urban regions. J. Geophys. Res. 104: 4065 – 4077

Satheesh SK, and Ramanathan V (2000) Large differences in tropical aerosol forcing at the top of the atmosphere and Earth's surface. Nature 405: 60 – 63

Saxena VK, and Menon S (1999) Sulfate-induced cooling in the Southeastern U.S.: An observational assessment. Geophys. Res. Lett. 26: 2489 – 2492

Schafer JS, Saxena VK, Wenny BN, Barnard W, and DeLuisi JJ (1996) Observed influence of clouds on ultraviolet-B radiation. Geophys. Res. Lett. 23: 2625 – 2628

Schwartz SE, Arnold F, Blanchet J-P, Durkee PA, Hoffman DJ, Hoppel WA, King MD, Lacis AA, Nakajima T, Ogren JA, Toon OB, and Wendisch M (1995) Group Report: Connections between aerosol properties and forcing of climate. In: Charlson RJ, Heintzenberg J (eds) Aerosol Forcing of Climate. John Wiley & Sons, Chichester, U.K.

Seckmeyer G, and McKenzie RL (1992) Elevated ultraviolet radiation in New Zealand (45˚S) contrasted with Germany (48˚N). Nature 359: 135 – 137

Stephens GL (1995) Review of atmospheric radiation: 1991 – 1994. Reviews of Geophysics, Supplement, pp.785 – 794

Ulman JC, and Saxena VK (1997) Impact of air mass histories on the chemical climate of Mount Mitchell, North Carolina. J. Geophys. Res. 102: 25451 – 25465

Varotsos CA, and Kondratyev KY (1995) On the relationship between total ozone and solar ultraviolet radiation at St Petersburg, Russia. Geophys. Res. Lett. 22: 3481 – 3484

Varotsos CA, Chronopoulos GJ, Katsikis S, and Sakellariou NK (1995) Further evidence of the role of air pollution on solar radiation reaching the ground. Int. J. Remote Sensing 16: 1883 – 1886

Waggoner AP, Weiss RE, Ahlquist NC, Covert DS, Will S, and Charlson RJ (1981) Optical characteristics of atmospheric aerosols. Atmos. Environ. 15: 1891 – 1909

Wang P, and Lenoble J (1994) Comparison between measurements and modeling of UV-B irradiance for clear sky: a case study. Appl. Opt. 33: 3964 – 3971

Wenny BN, Schafer JS, DeLuisi JJ, Saxena VK, Barnard WF, Petropavlovskikh IV, and Vergamini AJ (1998) A study of regional aerosol radiative properties and their effects on ultraviolet-B radiation. J. Geophys. Res. 103: 17083 – 17097

Whitby KY (1978) The physical characteristics of sulfur aerosols. Atmos. Environ. 12: 135 – 159

Wolff G (1981) Elemental carbon in the atmosphere. J. Air Pollut. Control Assoc. 31: 935 – 938

Yu SC, Zender CS, and Saxena VK (2001) Direct radiative forcing and atmospheric absorption by boundary layer aerosols in the southeastern US: model estimates on the basis of new observations. Atmos. Environ. 35: 3967 – 3977

Yuen P-F, Hegg DA, and Larsen TV (1994) The effects of in-cloud sulfate production on light scattering properties of continental aerosols. J. Appl. Meteorol. 33: 848 – 854